Electronic Supplementary Material (ESI) for Journal of Materials Chemistry C.

Supporting Information

1. Synthesis

1.1. Materials

2-methoxyethanol, p-toluenesulfonyl chloride (TsCl), triethylamine (NEt_3), 3-thiophenemethanol, 3-hexylthiophene, dichloro(1,3-bis(diphenylphosphino)propane)nickel ($Ni(dppp)Cl_2$) were purchased from Fluorochem. Sodium hydride (60% in mineral oil) (NaH), N-bromosuccinimide (NBS) and isopropyl magnesium chloride lithium chloride solution (1.3 M in THF) were purchased from Sigma-Aldrich. Dry tetrahydrofuran (THF) (99.5% over molecular sieves with AgroSeal) and dry dimethylformamide (DMF) (99.5% over molecular sieves with AgroSeal) were purchased from Acros Organics. All other solvents are HPLC grade purchased from Honeywell. All chemicals were used as purchased without further purification.

1.2. Synthesis of p-toluenesulfonyl methoxyethoxymethyl (1)

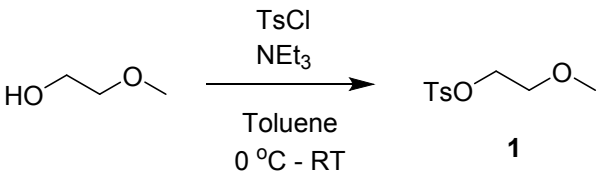

In a round bottom flask, p-toluenesulfonyl chloride (13.26 g, 77.02 mmol, 1.1 eq) was dissolved in toluene (125 mL) and the mixture was cooled to 0 °C. 2-Methoxyethanol (5.60 g, 70.80 mmol) was added dropwise, then immediately after, triethylamine (12.40 g, 122.50 mmol, 1.75 eq) was added dropwise. The reaction mixture was allowed to warm to RT and stir overnight, forming a cloudy suspension. The precipitate was filtered off, washed with toluene and the filtrate was concentrated under reduced pressure, The resulting yellow oil as the crude was purified by column chromatography, eluting with 1:1 diethyl ether to hexanes (Rf = 0.3) to give the product (**1**) (13.12 g, 56.99 mmol, 81 %) as a colourless oil. ^{1}H NMR (400 MHz, $CDCl_3$) δ 7.80 (d, J = 8.3 Hz, 2H), 7.34 (d, J = 8.2, 2H), 4.15 (t, J = 4.6 Hz, 2H), 3.57 (t, J = 4.8, 2H), 3.30 (s, 3H), 2.44 (s, 3H). ^{13}C NMR (100 MHz, $CDCl_3$) δ 145, 133, 130, 128, 70, 69, 59, 22, in accordance with literature.[1]

1.3. Synthesis of 3-(2-methoxyethoxy)methyl)thiophene (2)

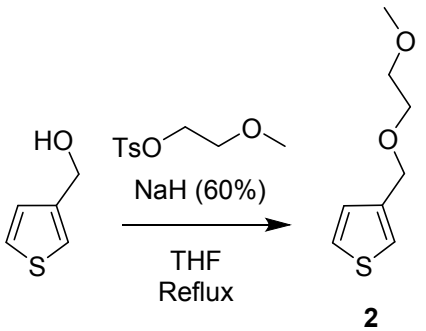

Sodium hydride (1.72 g, 60% in mineral oil, 43.10 mmol, 1.2 eq) was suspended in dry THF (350 mL) in an oven dried RBF with condenser under N_2 atmosphere. A vent needle was placed in the septum and 3-thiophenemethanol (4.09 g, 35.86 mmol) was added dropwise (yellow suspension). Once hydrogen stopped evolving, the vent needle was removed and 2-methoxyethyl p-toluenesulfonate (**1**) (8.98 g, 39.01 mmol, 1.1 eq) was added in one portion. The reaction was headed to reflux, stirring for 24 hours, then allowed to cool. The solid was filtered off, washed several times with diethyl ether and the yellow filtrate was transferred to a separating funnel. After washing organic layer with water (3 x 100 mL) and brine (2 x 200 mL), dried over $MgSO_4$ and concentrated under reduced pressure giving the crude as a yellow oil (5.63 g). The desired product was purified by a gradient column, starting with 1:4 ethyl ether in hexanes and eluting with 1:1 ethyl ether in hexanes (Rf = 0.34) to give the product (**2**) (2.93 g, 17.00 mmol, 48 %) as a yellow oil. ^{1}H NMR (400 MHz, $CDCl_3$) δ 7.28 (dd, *J* = 4.9, 1.96 Hz, 1H), 7.22 (m, 1H), 7.08 (dd, *J* = 5.0, 1.16 Hz, 1H), 4.58 (s, 2H), 3.62 - 3.54 (m, 4H), 3.89 (s, 3H). ^{13}C NMR (100 MHz, $CDCl_3$) δ 139.9, 127.3, 125.9, 122.8, 71.9, 69.1, 68.4, 59.0, in accordance with literature.[1]

1.4. Synthesis of 2,5-dibromo-3-(2-methoxyethoxy)methyl)thiophene (3)

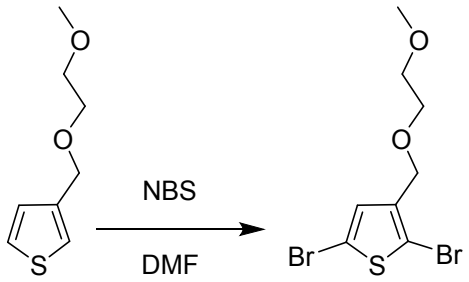

2 **3**

NBS (3.43 g, 19.27 mmol, 2.3 eq) was dissolved in dry DMF (125 mL) under nitrogen. The flask was covered to exclude light and cooled to 0 °C. 3-(2-(methoxyethoxy)methyl)thiophene (**2**) (1.45 g, 8.42 mmol) was added dropwise and the reaction was stirred at room temperature overnight (yellow solution). The reaction was quenched with H_2O (100 mL) and extracted with diethyl ether (3 x 100 mL), washed with H_2O (3 x100 mL), brine (100 mL) and dried over $MgSO_4$. Subsequent evaporation of solvent under reduced pressure and purification via column chromatography, eluting with 1:1 diethyl ether in hexanes (Rf = 0.62) gave the product (**3**) (1.94 g, 5.89 mmol, 86 %) as a yellow oil. ^{1}H NMR (400 MHz, $CDCl_3$) δ 6.99 (s, 1H), 4.43 (s, 2H), 3.61 - 3.53 (m, 4H), 3.38 (s, 3H). ^{13}C NMR (100 MHz, $CDCl_3$) δ 139, 131, 111, 110, 72, 69, 67, 59, in accordance with literature.[1]

1.5. Synthesis of 2,5-dibromo-3-hexylthiophene (4)

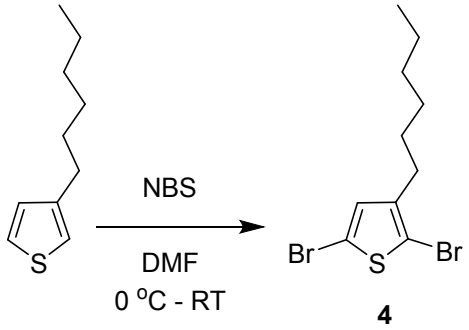

NBS (6.98 g, 39.06 mmol, 2.2 eq) was and dissolved in dry DMF (100mL) under a nitrogen atmosphere, covered from light and cooled to 0 °C. To this solution, 3-hexylthiophene (2.99 g, 17.75 mmol) was added dropwise allowed and then stirred overnight, allowing to reach RT (yellow solution). The solution was quenched with H_2O (100 mL) and the product was extracted with ethyl acetate (3 x 80mL). Combined organic layers were washed with H_2O (3 x 100 mL) and brine (100 mL), dried over anhydrous $MgSO_4$. Solvent evaporation and subsequent purification by column chromatography in hexanes (Rf = 0.64) yielded a colourless oil (5.22 g, 16.01 mmol, 90 %) as the product (**4**). ^{1}H NMR (400 MHz, $CDCl_3$) δ 6.78 (s, 1H), 2.50, (t, J = 7.6 Hz, 2H), 1.54 (quin, J = 6.4 Hz, 2H), 1.34 - 1.30 (m, 6H), 0.89 (t, J = 6.6 Hz, 3H). ^{13}C NMR (100 MHz, $CDCl_3$) δ 142, 130, 110, 107, 32, 30, 29, 26, 14, in accordance with literature.[2]

1.6. Synthesis of poly(3-hexylthiophene) (P3HT)

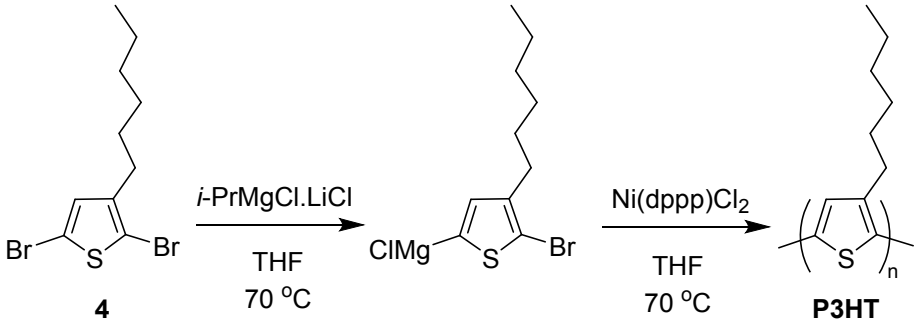

2,5-Dibromo-3-hexyl-thiophene (534 mg, 1.64 mmol) dissolved in dry THF (3.8 mL) in an oven dried microwave vial under nitrogen. It is paramount to ensure all glassware is dry to provide the highest yield. Added isopropyl magnesium chloride lithium chloride complex (1.3 M in THF, 1.2 mL, 0.98 eq) to a solution dropwise and the reaction mixture was stirred for 2 hr at 70 °C (dark yellow solution). This was then added to a suspension of $Ni(dppp)Cl_2$ (9 mg, 0.02 mmol, 1 mol%) in dry THF (3 mL), in a separate oven dried microwave vial and the polymerisation was stirred at 70 °C overnight. After cooling to room temperature, the reaction was terminated by addition of 1 mL of HCl (10 % (v/v)) followed again by stirring for 20 minutes. The mixture was added to cold well stirred methanol.

Obtained precipitates were Soxhlet extracted in methanol, acetone, hexane, and chloroform. The chloroform fraction was concentrated, reprecipitated in methanol and dried under vacuum at 40 °C to give the polymer (181 mg, 68 %) as a brown solid. ^{1}H NMR (400 MHz, $CDCl_3$) δ 6.98 (s, 1H), 2.80 (t, *J* = 7.8 Hz, 2H), 1.71 (quin, *J* = 8.2 2H), 1.45 - 1.33 (m, 6H), 0.91 (t, *J* = 6.9 Hz, 3H). GCP ($CHCl_3$): Mn = 30.0 kg mol^{-1}, Mw = 41.2 kg mol^{-1}, PDI = 1.38.

1.7. Synthesis of P(3HT:3MEMT) co-polymers

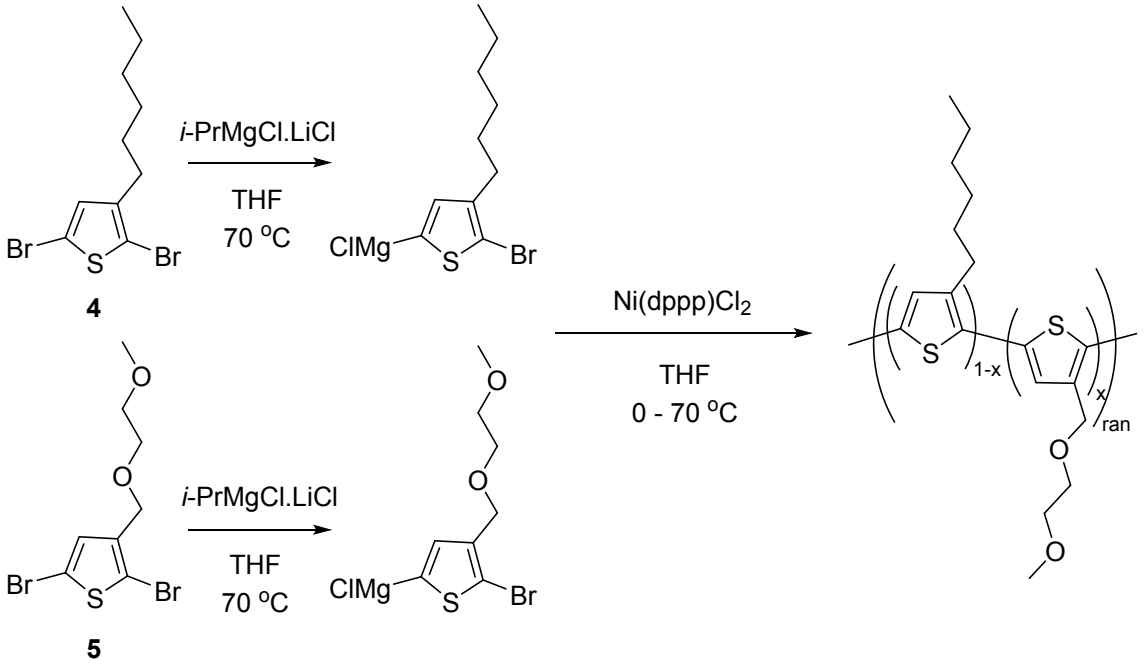

1.7.1. P5 (x = 0.05)

Two separate microwave vials were charged with 2,5-dibromo-3-(2-(methoxyethoxy)methyl)thiophene (**4**) (133.5 mg, 0.40 mmol, 0.05 eq) and 2,5-dibromo-3-hexylthiophene (**5**) (2.51 g, 7.68 mmol, 0.95 eq) and each dissolved in dry THF (10 mL) under a nitrogen atmosphere. Isopropylmagnesium chloride lithium chloride (1.3 M in THF, 5.6 mL, 7.28 mmol) was added dropwise to the 2,5-dibromo-3-hexylthiophene solution and (1.3 M in THF, 0.29 mL, 0.38 mmol) to the 2,5-dibromo-3-(2-(methoxyethoxy)methyl)thiophene solution and the reactions were heated to 70 °C for 2 hrs. The solutions were combined into one vessel at 0 °C as not to initiate polymerisation and a suspension of Ni(dppp)Cl_2 (43.8 mg, 0.08 mmol, 1 mol%), in dry THF (10 mL) was added in one portion. The polymerisation was heated to 70 °C overnight then cooled to room temperature and quenched with 1mL of HCl (10% (v/v)). After precipitating in methanol, Soxhlet extraction was performed using methanol, acetone, hexane and chloroform. The chloroform fraction was concentrated under reduced pressure, reprecipitated in methanol and dried under vacuum at 40 °C

to give the polymer (**P5**) (920.6 mg, 76%) as a brown solid. ^{1}H NMR (400 MHz, $CDCl_3$) δ 7.28 (s, 0.02H), 7.03 – 6.98 (m, 1H), 4.67 – 4.43 (m, 0.09H), 3.72 - 3.57 (m, 0.19H), 3.43 – 3.39 (s, 0.14H), 2.83 – 2.57 (m, 2H), 1.71 (quin, *J* = 8.0 Hz, 2H), 1.46 – 1.34 (m, 6H), 0.92 (t, *J* = 8.0 Hz, 3H). GCP ($CHCl_3$): Mn = 31.0 kg mol^{-1}, Mw = 47.6 kg mol^{-1}, PDI = 1.54.

1.7.2. P10 (x = 0.1)

Following the polymerisation procedure above with 2,5-dibromo-3-(2-(methoxyethoxy)methyl)thiophene (**4**) (280.7 mg, 0.85 mmol, 0.1 eq) and 2,5-dibromo-3-hexylthiophene (**5**) (2.51 g, 7.68 mmol, 0.9 eq) with isopropyl magnesium chloride lithium chloride complex (1.3M in THF) added to each (0.6 mL, 0.81 mmol, 0.98 eq and 5.6 mL, 7.28 mmol, 0.98 eq respectively). Added Ni(dppp)Cl_2 (43.4 mg, 0.09 mmol, 1 mol%) to combined solutions to afford product (**P10**) (1.09 g, 77 %) as a brown solid. ^{1}H NMR (400 MHz, $CDCl_3$) δ 7.28 (s, 0.04H), 7.07 – 6.98 (m, 1H), 4.67 – 4.43 (m, 0.22H), 3.72 - 3.57 (m, 0.46H), 3.43 – 3.37 (s, 0.34H), 2.82 – 2.57 (m, 2H), 1.71 (quin, *J* = 8.0 Hz, 2H), 1.44 – 1.34 (m, 6H), 0.90 (t, *J* = 8.0 Hz, 3H). GCP ($CHCl_3$): Mn = 38.2 kg mol^{-1}, Mw = 57.4 kg mol^{-1}, PDI = 1.50.

1.7.3. P20 (x = 0.2)

Following the polymerisation procedure above with 2,5-dibromo-3-(2-(methoxyethoxy)methyl)thiophene (**4**) (584.3 mg, 1.77 mmol, 0.2 eq) and 2,5-dibromo-3-hexylthiophene (**5**) (2.31 g, 7.08 mmol, 0.8 eq) with isopropyl magnesium chloride lithium chloride complex (1.3M in THF) added to each (1.3 mL, 1.68 mmol, 0.98 eq and 5.2 mL, 6.73 mmol, 0.98 eq respectively). Added Ni(dppp)Cl_2 (39.4 mg, 0.07 mmol, 1 mol%) to combined solutions to afford product (**P20**) (1.11g, 75 %) as a brown solid. ^{1}H NMR (400 MHz, $CDCl_3$) δ 7.28 (s, 0.16H), 7.03 – 6.98 (m, 1H), 4.67 – 4.43 (m, 0.5H), 3.63 - 3.61 (m, 1H), 3.42 – 3.39 (s, 0.76H), 2.82 – 2.57 (m, 2H), 1.71 – 1.69 (m, 2H), 1.42 – 1.29 (m, 6H), 0.93 – 0.90 (m, 3H). GCP ($CHCl_3$): Mn = 18.2 kg mol^{-1}, Mw = 52.7 kg mol^{-1}, PDI = 2.90.

1.7.4. P30 (x = 0.3)

Following the polymerisation procedure above with 2,5-dibromo-3-(2-(methoxyethoxy)methyl)thiophene (**4**) (423.2 mg, 1.28 mmol, 0.3 eq) and 2,5-dibromo-3-hexylthiophene (**5**) (974.4 g, 2.99 mmol, 0.7 eq) with isopropyl magnesium chloride lithium chloride complex (1.3M in THF) added to each (0.94 mL, 1.22 mmol, 0.98 eq and 2.18 mL, 2.84 mmol, 0.98 eq respectively). Added Ni(dppp)Cl_2 (23.2 mg, 0.04 mmol, 1 mol%) to combined solutions to afford product (**P30**) (399.4 mg, 56 %) as a brown solid. ^{1}H NMR (400 MHz, $CDCl_3$) δ 7.28 (s, 0.22H), 7.03 – 6.98 (m, 1H), 4.67 – 4.43 (m, 0.92H), 3.72 - 3.62 (m, 1.88H), 3.43 – 3.39 (s, 1.38H), 2.83 – 2.57 (m, 2H),

1.71 – 1.69 (m, 2H), 1.44 – 1.34 (m, 6H), 0.93 – 0.88 (m, 3H). GCP ($CHCl_3$): Mn = 22.8 kg mol^{-1}, Mw = 31.7 kg mol^{-1}, PDI = 1.39.

1.8. Synthesis of potassium 2,3,5,6-tetrafluoro-7,7,8,8-tetracyanoquinodimethane (KF4TCNQ)

Separate solutions of potassium iodide (28 mg, 0.17 mmol, 1.5 eq) in dry acetonitrile (1.5 mL) under nitrogen and a solution of 2,3,5,6-tetrafluoro-7,7,8,8-tetracyanoquinodimethane (F4TCNQ) (31 mg, 0.11 mmol, 1 eq) in dry acetonitrile (1.5 mL) under nitrogen were cooled to 0 °C. The cooled solution of potassium iodide was then added dropwise to the solution of F4TCNQ and stirred at 0 °C for 30 mins. The solid was then filtered off and washed with cold acetonitrile (15 mL) and then cold diethyl ether (15 mL). The resulting solid was then dried under vacuum at 40 °C for 20 minutes to afford the product as a blue solid (22 mg, 63 %). FTIR (v/cm^{-1}): CN = 2191, 2209, in accordance with the literature.[3]

2. Characterisation

2.1. Nuclear Magnetic Resonance (NMR)

^{1}H and ^{13}C NMR spectroscopy was carried out on a Bruker AV400 or Bruker AVIII400 spectrometer. Deuterated solvents we purchased from Cambridge isotopes. Samples were dissolved in $CDCl_3$ between 0.4 – 0.6 mL. Polymer samples were heated with heat gun to dissolve solution using ~5 mg in $CDCl_3$.

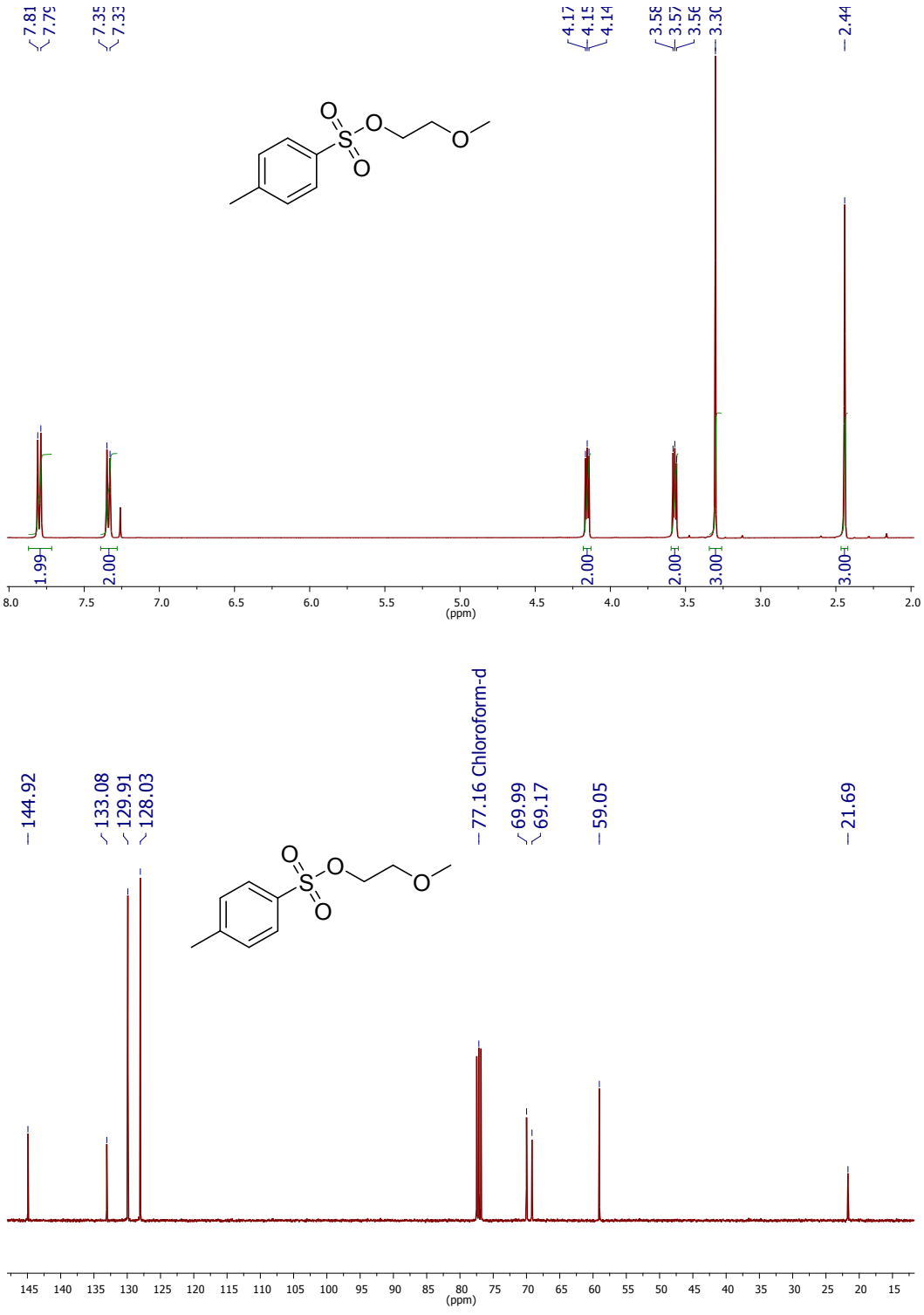

Figure S1. ^{1}H NMR (top) and ^{13}C NMR (bottom) of p-toluenesulfonyl methoxyethoxymethyl (**1**) in $CDCl_3$. NMRs were compared to previous literature.[1]

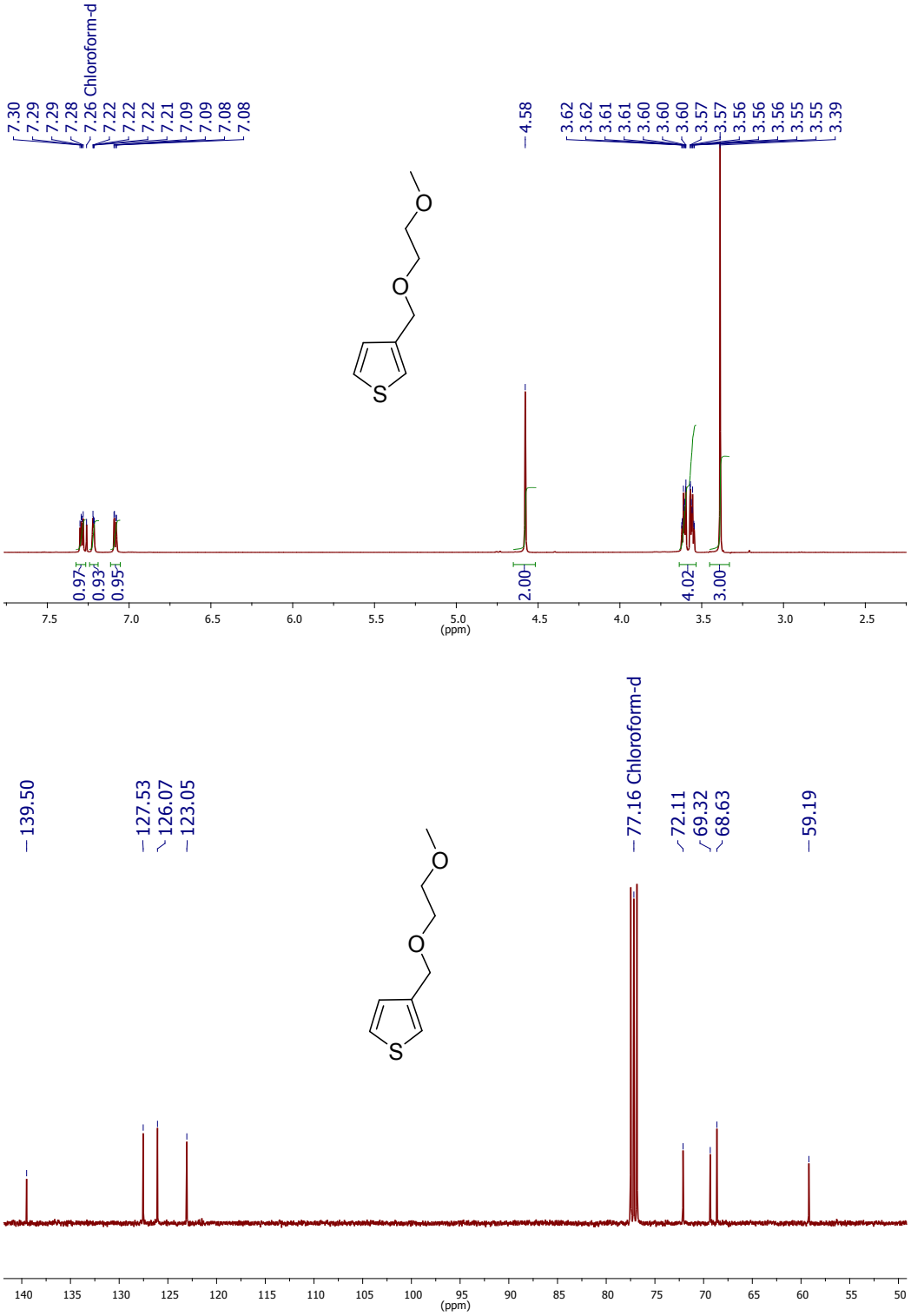

Figure S2. ^{1}H NMR (top) and ^{13}C NMR (bottom) of 3-(2-methoxyethoxy)methyl)thiophene (**2**) in $CDCl_3$. NMRs were compared to previous literature.[1]

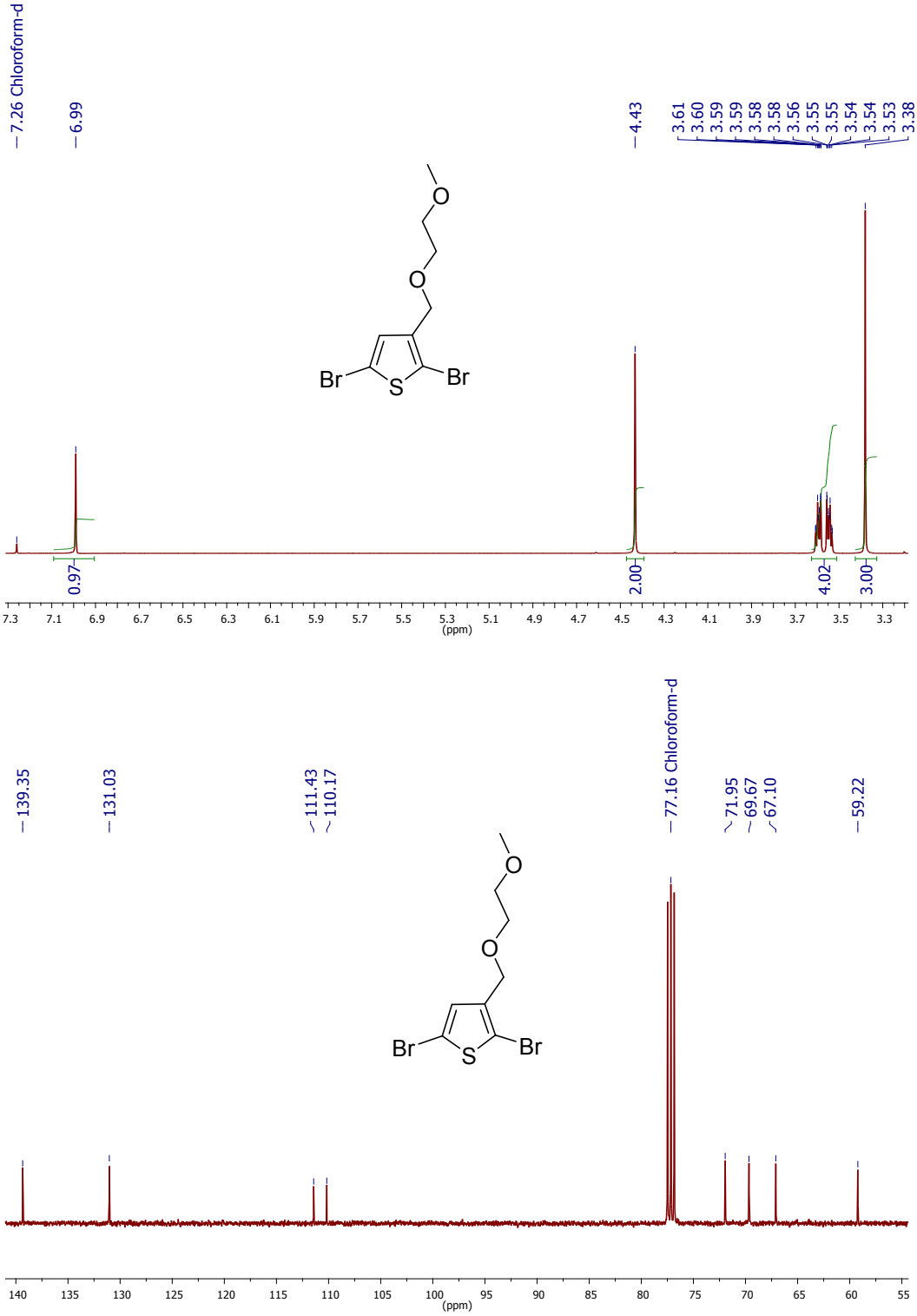

Figure S3. ^{1}H NMR (top) and ^{13}C NMR (bottom) of 2,5-dibromo-3-(2-methoxyethoxy)methyl)thiophene (**3**) in $CDCl_3$. NMRs were compared to previous literature.[1]

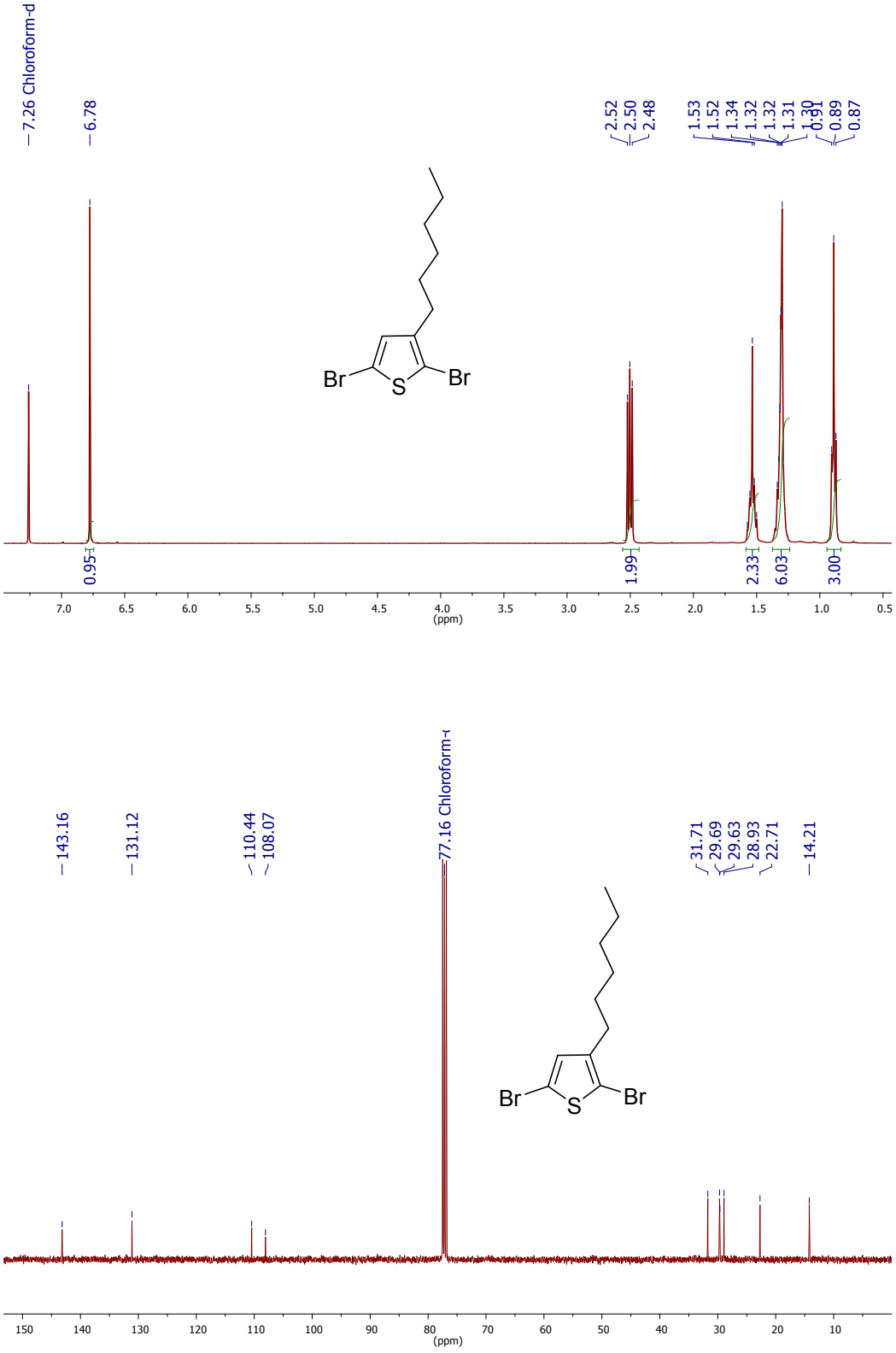

Figure S4. ^{1}H NMR (top) and ^{13}C NMR (bottom) of 2,5-dibromo-3-hexylthiophene (**4**) in $CDCl_3$. NMRs were compared to previous literature.[2]

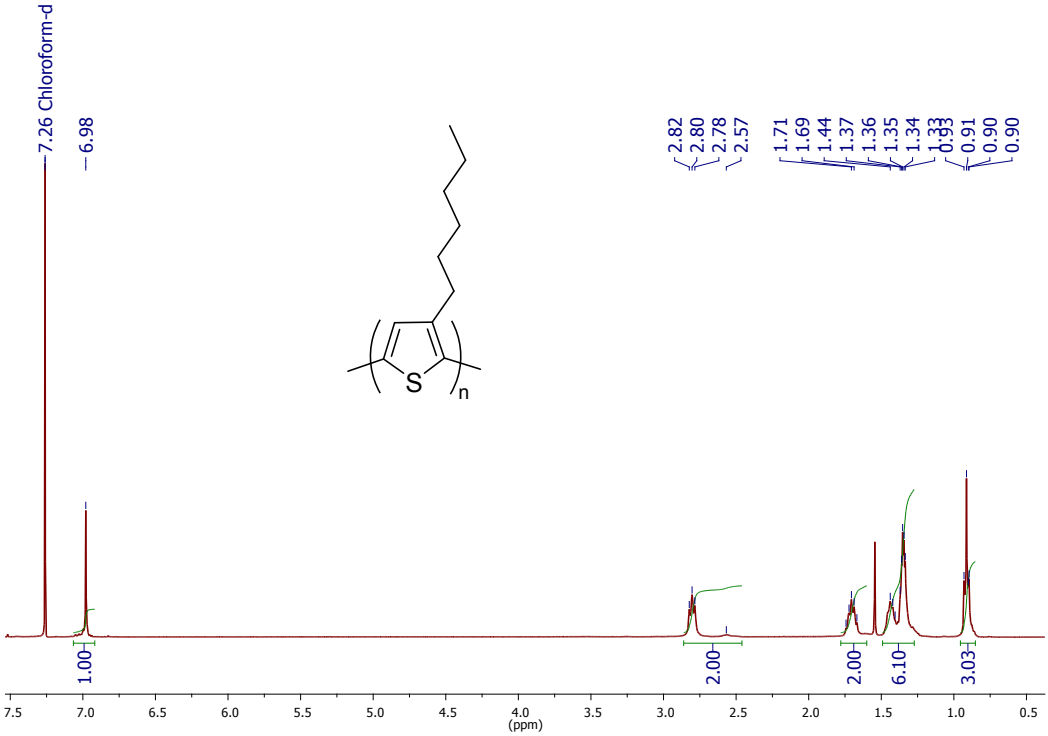

Figure S5. ^{1}H NMR of **P3HT** in $CDCl_3$. Triplet at 2.80 ppm and broad peak at 2.57 ppm are from the alpha protons on the alkyl chain and the integrated ratio between these peaks indicates the head to tail content/regioregularity.[4]

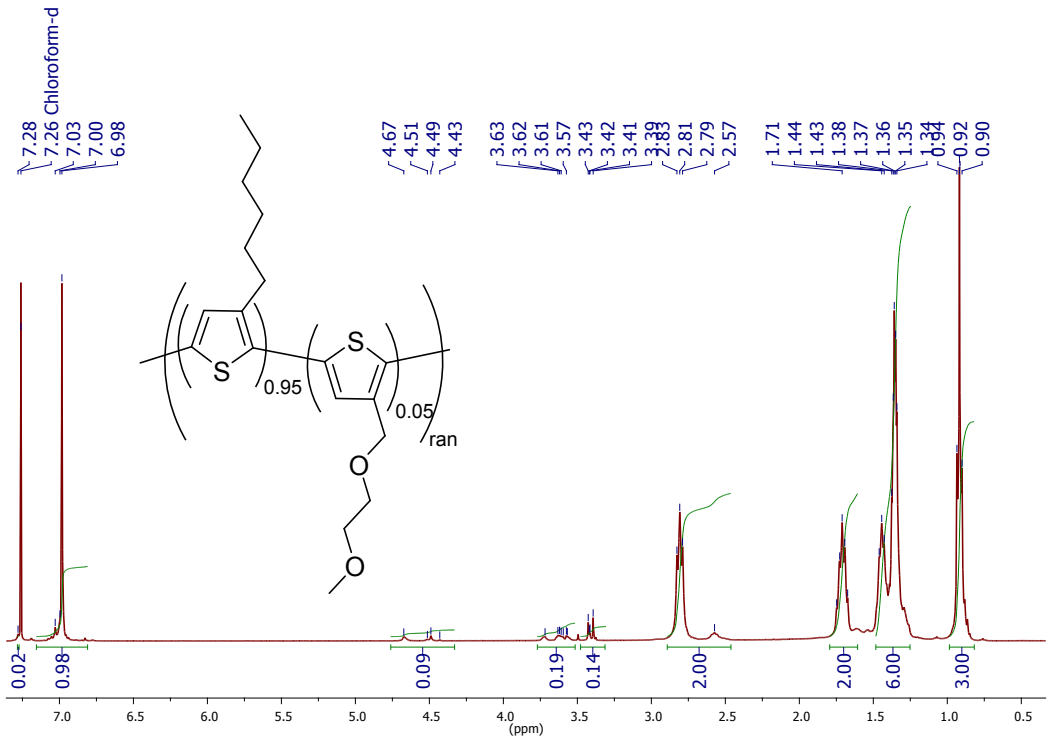

Figure S6. ^{1}H NMR of **P5.**

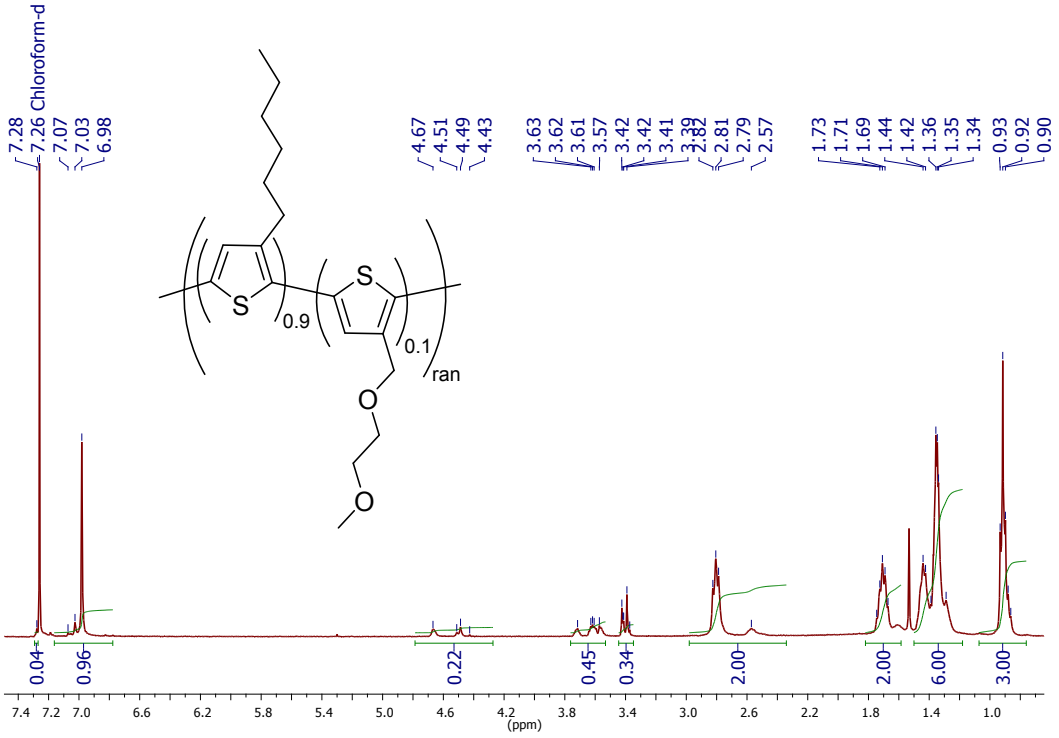

Figure S7. ^{1}H NMR of **P10.**

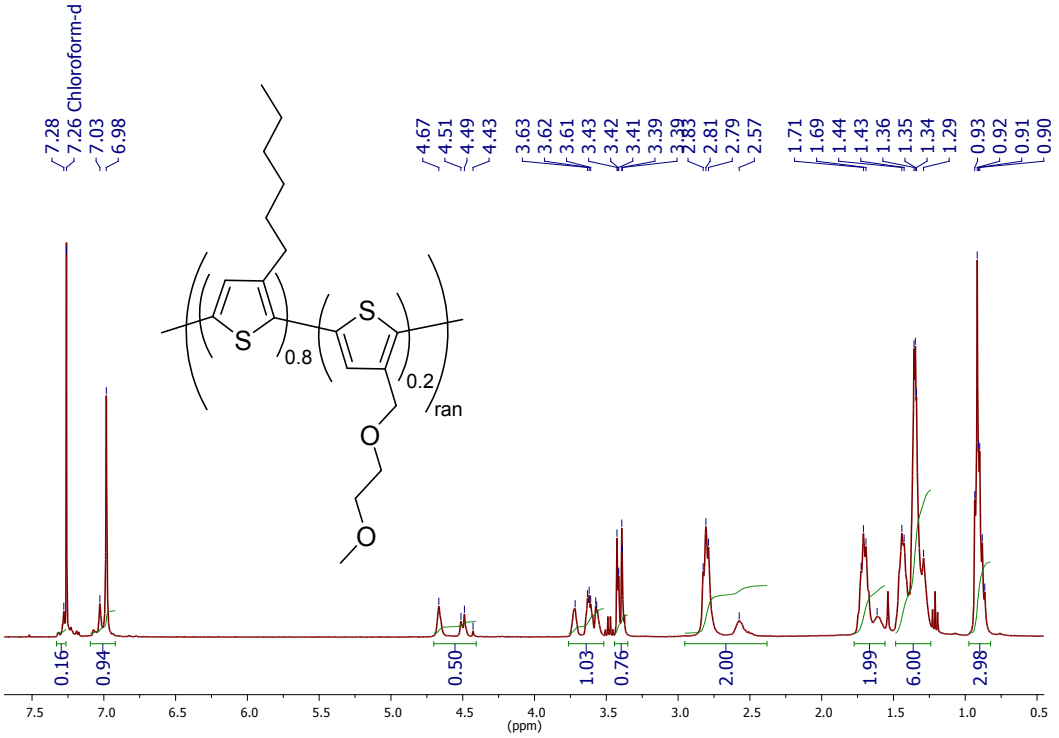

Figure S8. ^{1}H NMR of **P20.**

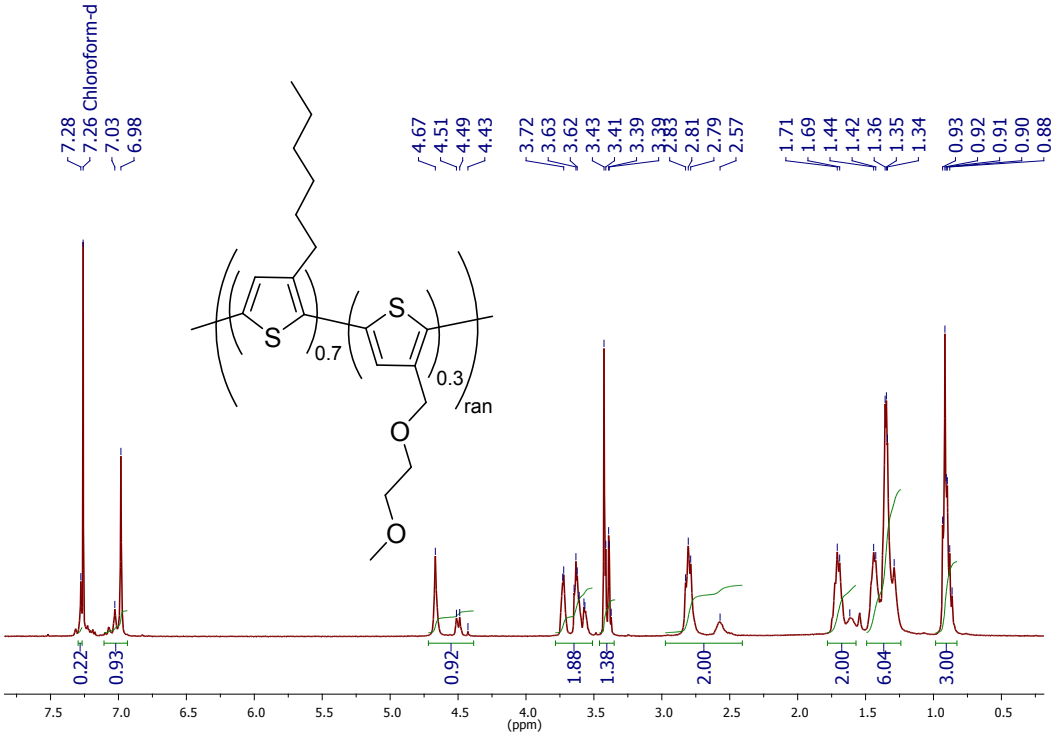

Figure S9. ^{1}H NMR of **P30.**

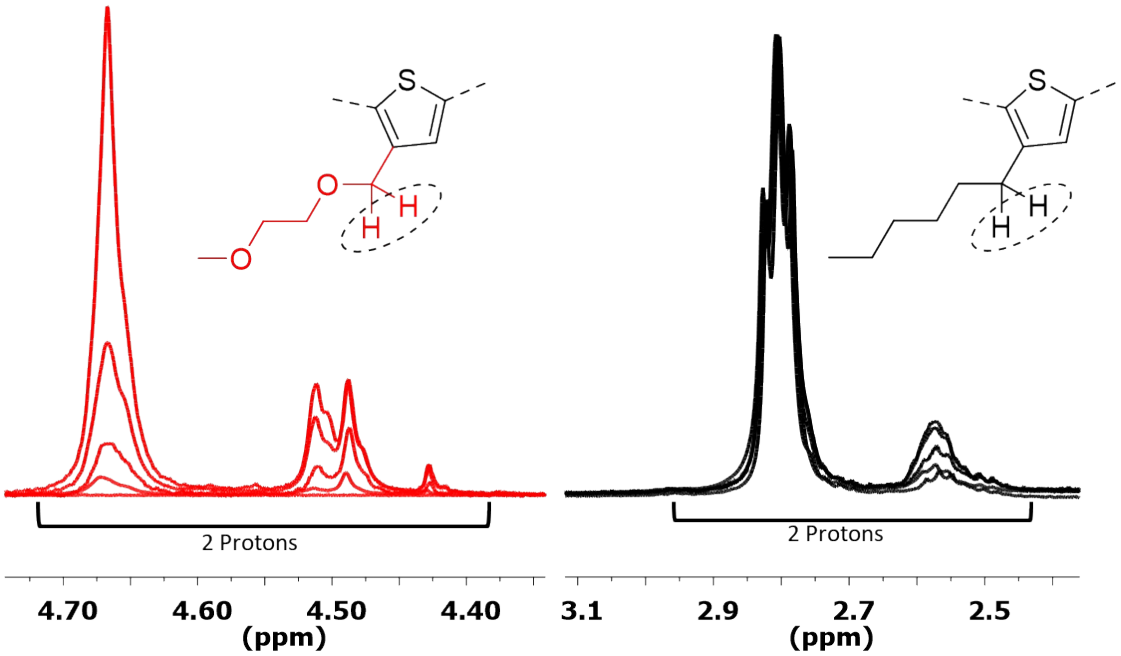

Figure S10. Overlapped ^{1}H NMR showing the alpha protons from alkyl (3.1 – 2.4 ppm) and polar (4.8 – 4.3 ppm) side chains from P3HT and co-polymers **P5** – **P30**.

Table S1. Calculation of monomer ratio of polymer ratio from ^{1}H NMR spectrum.

Polymer	Alkyl Integration[a]	Polar Integration[b]	Total	Polar Ratio[c]
P5	2.00	0.09	2.09	0.04
P10	2.00	0.22	2.22	0.10
P20	2.00	0.50	2.50	0.20
P30	2.00	0.92	2.92	0.32

[a]Between 3.1 – 2.4 ppm. [b]Between 4.8 – 4.3 ppm. [c]Calculated by polar ratio = (polar integration)/(total).

2.2. Gel Permeation Chromatography (GPC)

GPC was carried out using Shimadzu Prominence GPC system, comprised of a SIL-20A auto sampler, LC-20AT liquid chromatograph, CTO-20A column oven, RID-20A refractive index detector and an SPD-20A UV-Vis detector. HPLC grade chloroform stabilised with amylene was purchased from Acros Organics. Analysis was carried out on Shimadzu's LabSolutions software.

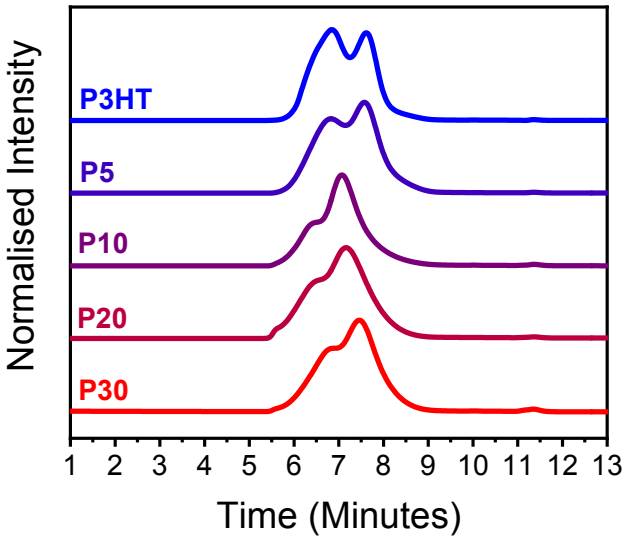

Figure S11. Stacked GPC traces of P3HT and **P5 – P30**. Molecular weight distributions were obtained from the integration of the whole peak.

2.3. Thermogravimetric Analysis (TGA) and Differential Scanning Calorimetry (DSC)

TGA was carried out on a TA instruments Q500 using a platinum pan at 10 °C/min between 25 - 800 °C under nitrogen then 800 – 1000 °C under air. Between 0.5 – 3 mg of polymer was used for TGA. DSC was carried out on TA Instruments DSC25 running at 10 °C/min. Between 1 – 5 mg of polymer was used for DSC.

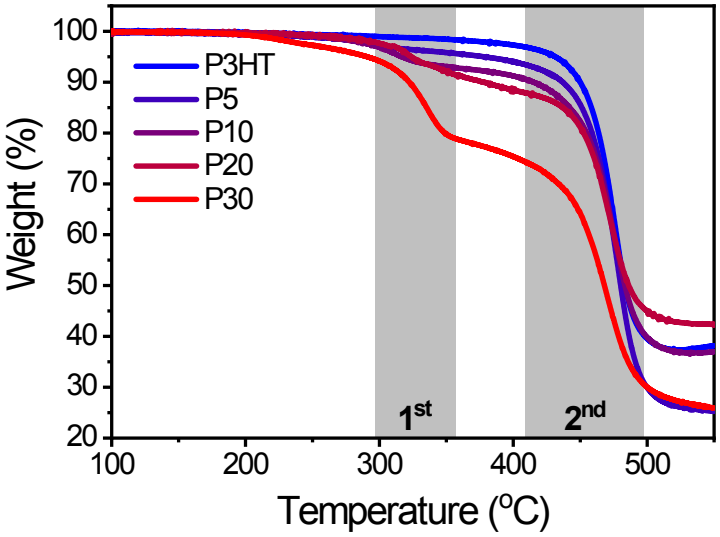

Figure S12. Overlaid TGA thermograms of P3HT and **P5 – P30**. Greyed areas illustrate the 1st and 2nd onset of degradation. The event at 200 °C for **P30** is attributed to residual solvent/water.

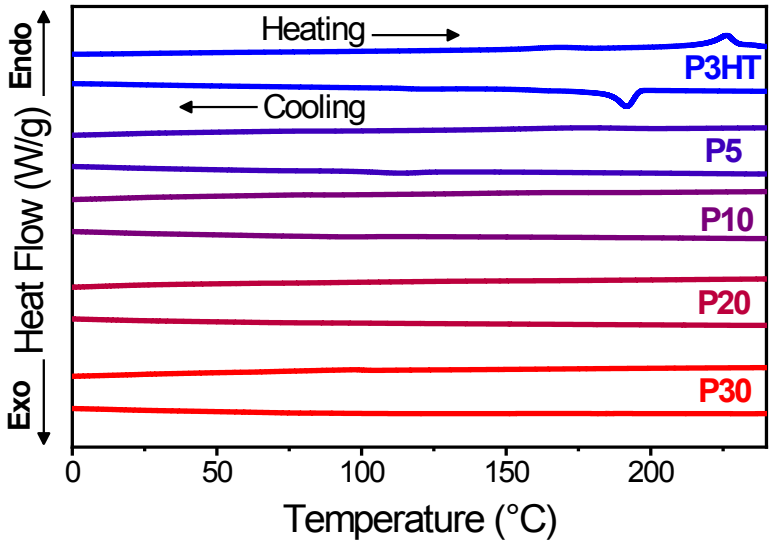

Figure S13. DSC thermograms of **P3HT** and co-polymers **P5** – **P30**. The second cycle is shown for DSC.

Table S2. Table showing the thermal properties from TGA and DSC measurements.

Polymer	1st Onset of Degradation (°C)[a]	2nd Onset of Degradation (°C)[b]	T_c (°C)	T_m (°C)
P3HT	N/A	456	192	226
P5	271	459	N/A	N/A
P10	290	453	N/A	N/A
P20	312	450	N/A	N/A
P30	313	444	N/A	N/A

[a]Attributed to increasing polar monomer content within co-polymers. [b]Attributed to the alkyl monomer content.

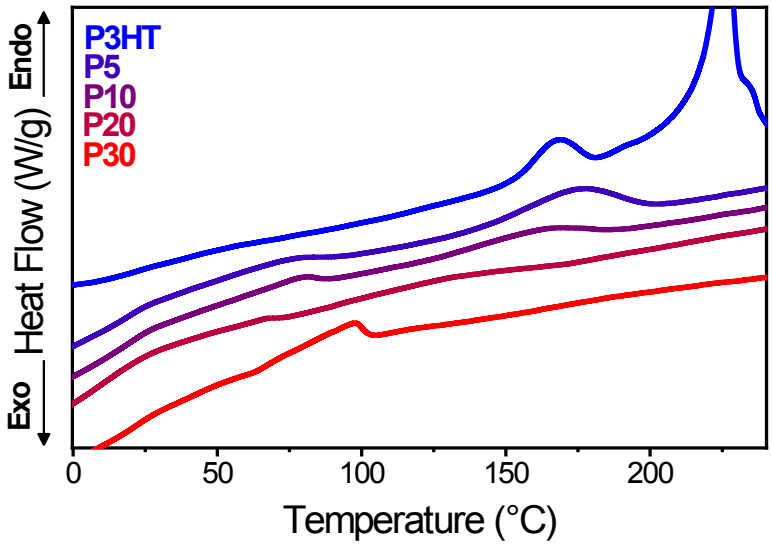

Figure S14. Zoomed DSC thermograms of P3HT and co-polymers **P5** – **P30** showing the heating cycle of the second cycle.

2.4. Ultraviolet-visible (UV-Vis) Spectroscopy of undoped Films

UV-Vis spectroscopy was carried out on Shimadzu UV3600 UV-Vis-NIR spectrometer. Solution UV-Vis was carried out in quartz cuvettes from solutions of polymers in o-dichlorobenzene (ODCB) at 0.01 mg/ml at RT. Thin film UV-Vis was carried out by spin coating thin films onto quartz microscope slides from 10 mg/ml polymer solutions in ODCB dissolved at 80 °C. Solutions were spun at 2000 rpm for 90 secs then 8000 rpm for 30 secs from 80 °C in air on a Laurell Technologies Corporation Model WS-650MZ-23NPPB spin coater. Quartz slides were cleaned by sonicating in soapy water, DI water, acetone, and IPA for 15 mins. Prior to spin coating substrates were plasma cleaned using a Harrick Plasma PDC-32G plasma cleaner for 30 mins.

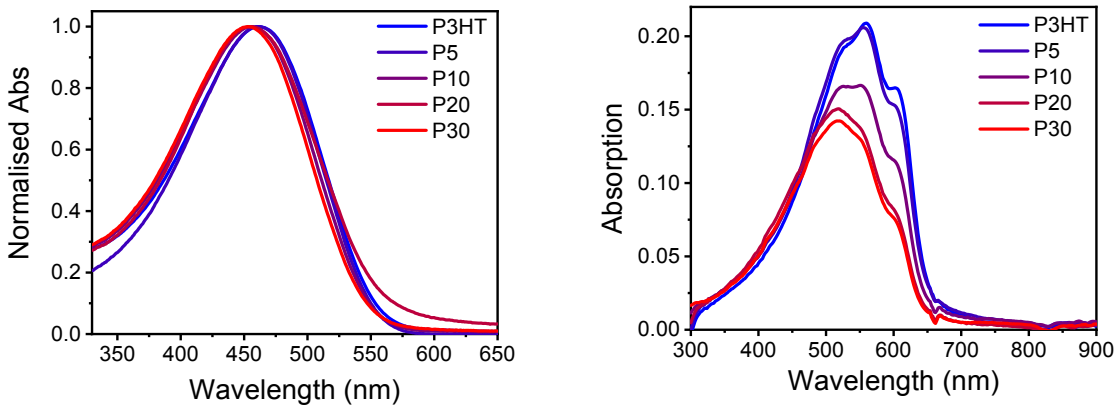

Figure S15. Normalised solution (left) and thin film (right) UV-Vis spectra of **P3HT** and **P5** – **P30**.

Table S3. Thickness measurements of polymer thin films spun from 10 mg/ml ODCB solutions at 80 °C at 2000 rpm for 90 secs.

Polymer	Measurement 1 (nm)	Measurement 2 (nm)	Measurement 3 (nm)	Average (nm)	Error (nm)
P3HT	30	29	32	30	± 1.5
P5	32	29	27	29	± 2.5
P10	30	28	31	30	± 1.5
P20	25	26	33	28	± 4.4
P30	25	27	28	27	± 1.5

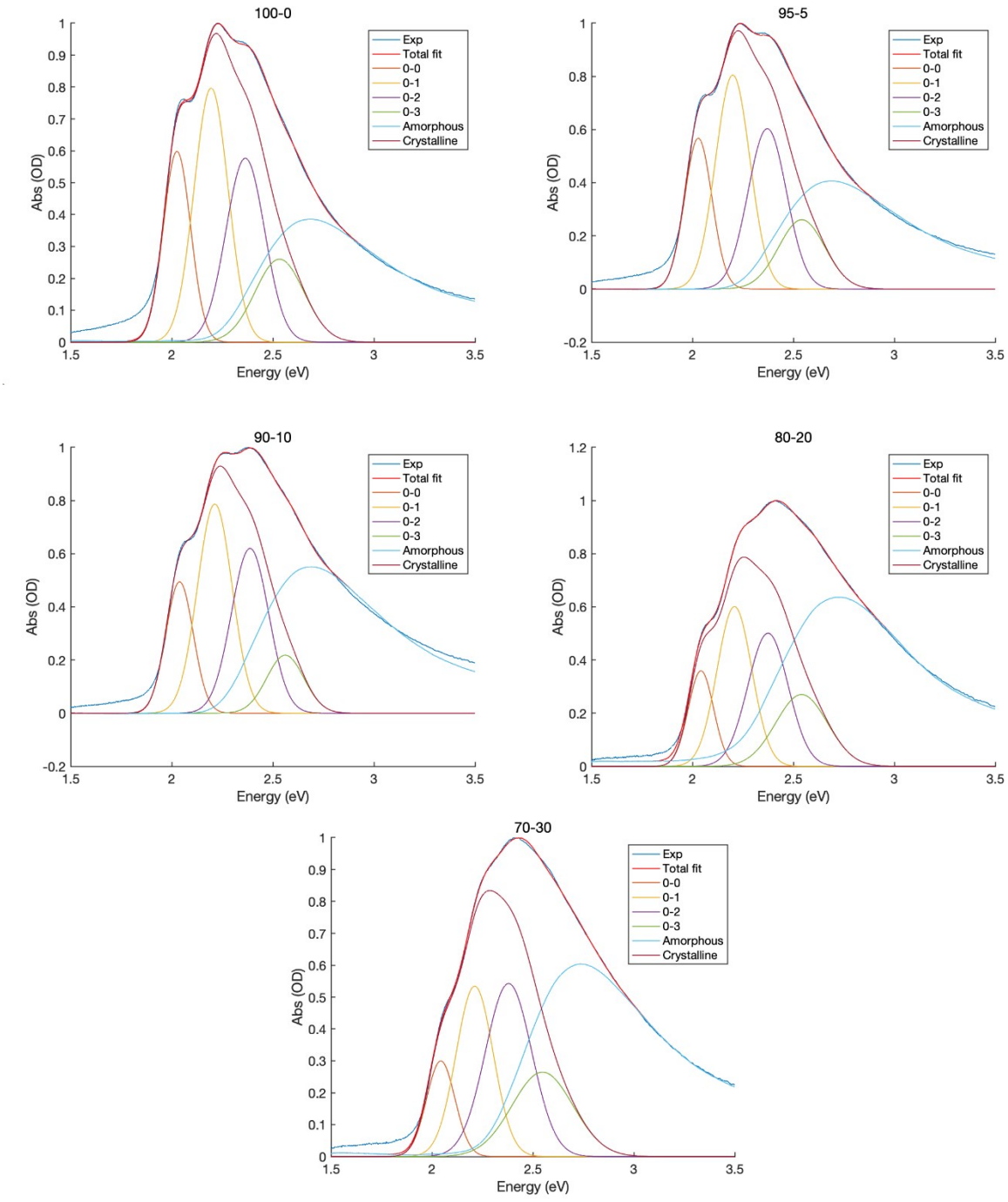

Figure S16. Fitted normalised thin film UV-vis spectra of P3HT (labelled 100-0), **P5** (95-5), **P10** (90-10), **P20** (80-20) and **P30** (70-30). The fit function uses 4 Gaussians to fit the vibronic progression within the crystalline regions, and the solution-state UV-Vis spectrum (**Figure S13**) to approximate the amorphous regions. The fitting function is

$$A(E) = a_{am}A_{sol}(E) + \sum_{n=0}^{3} a_n e^{-4ln(2)\left(\frac{E-(E_{0-0}+nE_p)}{w_n}\right)^2} \qquad (1)$$

where a_n is absorption intensity of mode n, a_{am} is the intensity of the amorphous region, $A_{sol}(E)$ is the experimental solution-state UV-vis spectrum, $E_{0\text{-}0}$ is the energy of the 0-0 transition, n is the vibrational energy level of the excited state, E_p is the energy of the coupled vibrational mode (typically ~145 cm^{-1} = 0.18 eV) and w_n is the full width at half maximum of the nth vibronic feature. In total there are 11 fit parameters: a_s, a_n, b_0, b_{prog}, and c_n, for n=0-4.

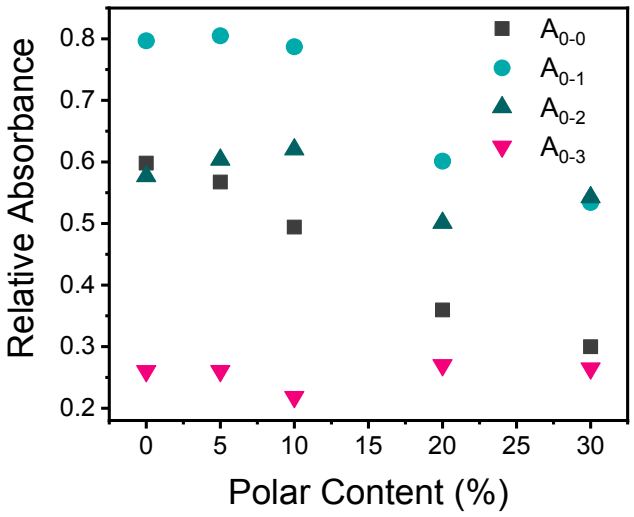

Figure S17. Absorption height of the four vibronic fitted Gaussian peaks in the crystalline region of the thin film UV-Vis spectra.

2.5. Cyclic Voltammetry (CV)

CV was carried out using a PalmSens EmStat3 potentiostat with degassed MeCN with 0.1 M tetrabutyl hexafluorophosphate as the electrolyte measured at 50, 100 and 200 mV/s scan rate. The reference, counter and working electrode were Ag/Ag^+, platinum and glassy carbon, respectively. Thin films were drop cast from 1 mg/ml chloroform solutions onto glassy carbon electrode. Ferrocene was used as the standard was measure using 0.01 M ferrocene in degassed MeCN with 0.1 M tetrabutyl hexafluorophosphate as supporting electrolyte at a scan rate of 50, 100 and 200 mV/s.

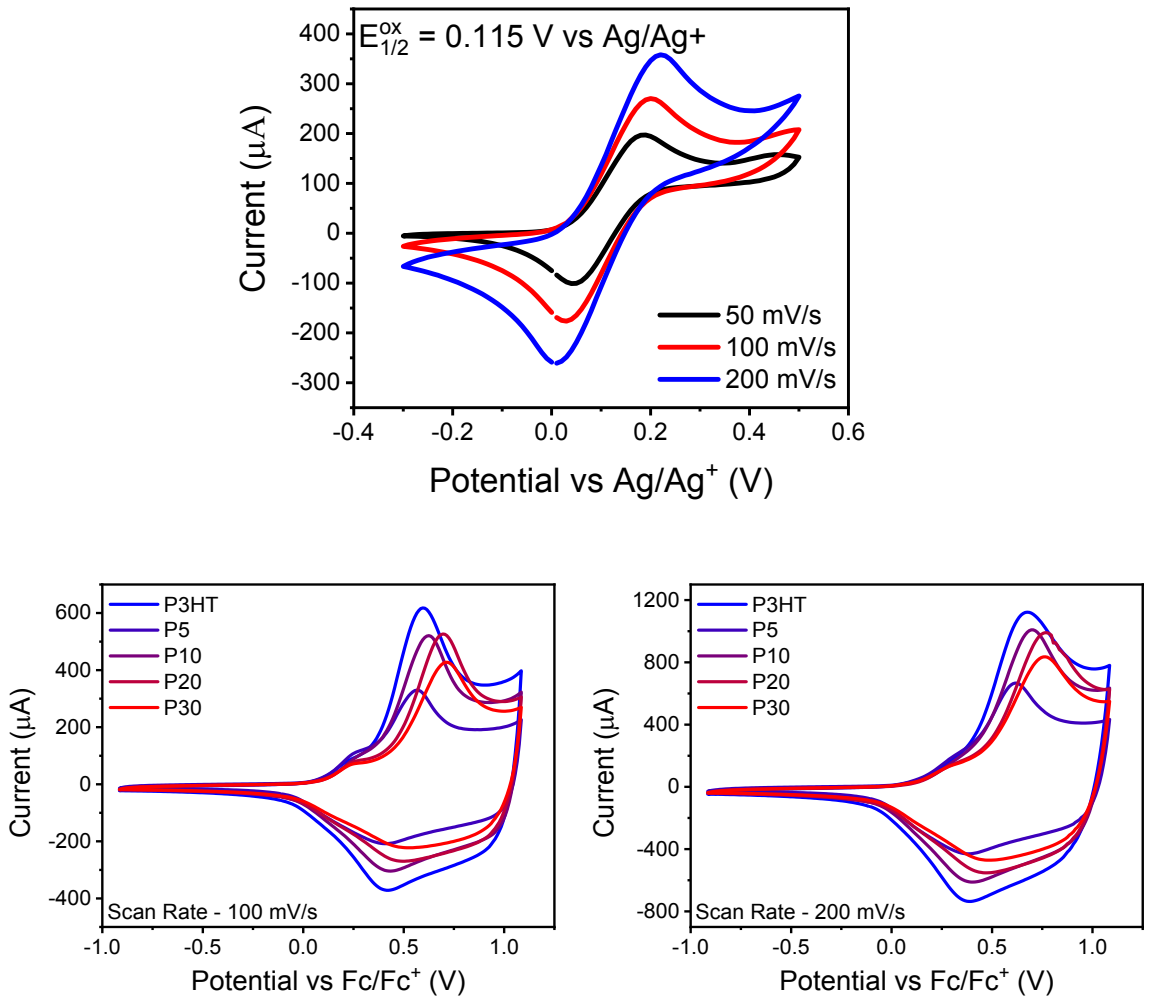

Figure S18. Cyclic voltammograms of 0.01 M Ferrocene in MeCN (top) and thin films of P3HT and co-polymers with a scan rate of 100 mV/s (bottom left) and 200 mV/s (bottom right).

2.6. Density Functional Theory (DFT) Calculations

DFT calculations were carried out using B3LYP/6-31g(d,p) basis set in the gas phase and visualised using Avogadro version 1.2.0.

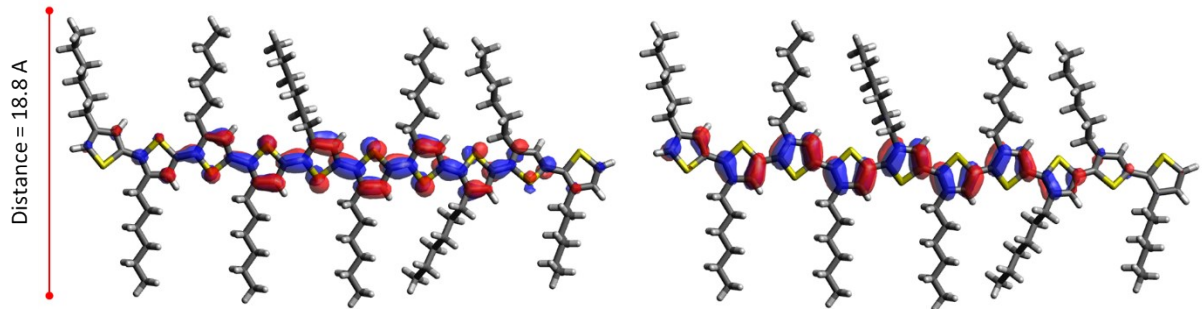

Figure S19. Optimised structure of 10 monomer units of **P3HT** with HOMO (left) and LUMO (right) overlaid. The calculated HOMO and LUMO have values of -4.63 and -2.54 eV respectively.

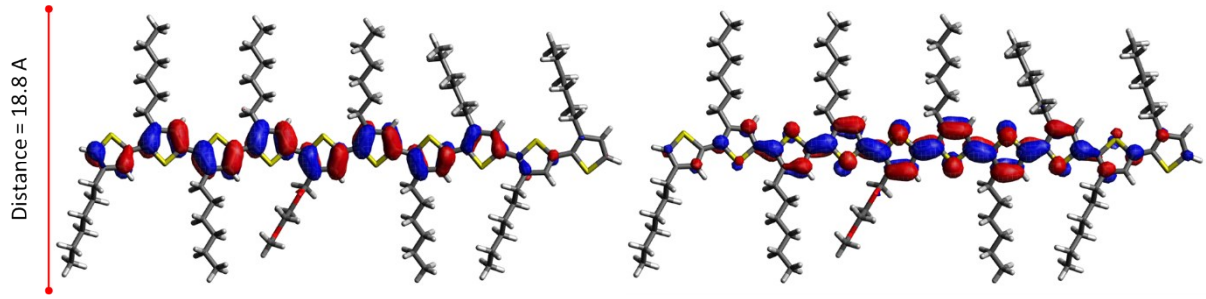

Figure S20. Optimised structure of 10 monomer units of **P10** with HOMO (left) and LUMO (right) overlaid. One polar unit is placed in the middle. The calculated HOMO and LUMO have values of -4.67 and -2.54 eV respectively.

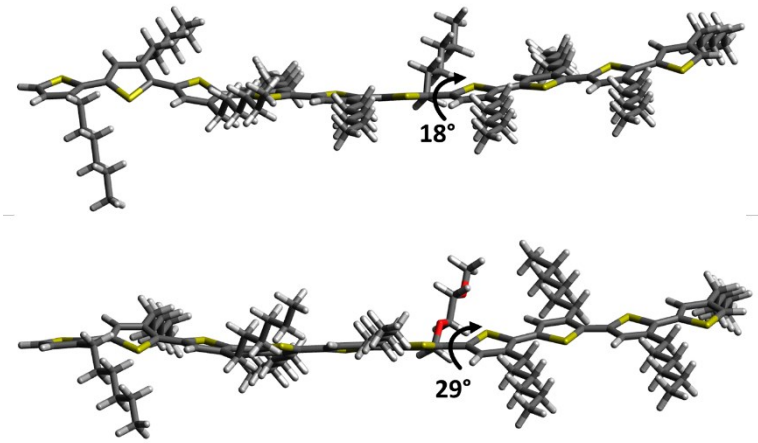

Figure S21. Side on view of optimised polymer structures of 10 monomer units of P3HT (top) and **P10** (bottom). The SCCS dihedral angle is indicated by the arrow.

2.7. X-Ray Diffraction (XRD) and Grazing Incidence Wide Angle Scattering (GIWAXS)

XRD was carried out on PANalytical X'Pert Pro diffractometer using Cu K_α X-rays, setup in grazing incidence configuration. Thin films were drop cast onto boron doped single side polished silicon substrates of <100> orientation, purchased form PI-KEM, from 10 mg/ml polymer solutions in ODCB. Films were covered with glass petri dish and allowed to dry overnight in air. GIWAXS measurements were carried out at beamline 8-ID-E of the Advanced Photon Source, Argonne National Laboratory with 10.92 keV synchrotron radiation under vacuum at room temperature. The incident angle of the X-ray beam relative to the polymer film was set at 0.14°, and the scattering signal was collected by a Pilatus 1MF pixel array detector 228.165 mm away from the sample with the integration time of 5s. Data was processed with the GIXSGUI package for MATLAB and line cuts were fit with custom MATLAB code.[5] GIWAXS thin film samples were spun onto silicon substrates from 10 mg/ml ODCB solutions at 1500 rpm for 90 secs. All silicon slides were cleaned by sonicating in soapy water, DI water, acetone,

and IPA for 15 mins. Prior to spin coating substrates were plasma cleaned using a Harrick Plasma PDC-32G Plasma Cleaner for 30 mins. Polymer thin films were doped with F4TCNQ using high and low doping conditions under a nitrogen atmosphere in a MBRAUN LABstar glove box on a Chemat Scientific KW-4A spin coater. High doping was carried out by depositing a 1 mg/ml solution of F4TCNQ in MeCN, leaving on the films for 60 secs, then removed via spinning at 5000 rpm for 30 secs. A second 1 mg/ml solution of F4TCNQ in ODCB was deposited, left on for 60 secs and then spun off at 8000 rpm for 30 secs. Low doping was carried out via depositing a 0.1 mg/ml solution of F4TCNQ in MeCN, leaving on for 10 secs, then spinning off at 8000 rpm for 30 secs.

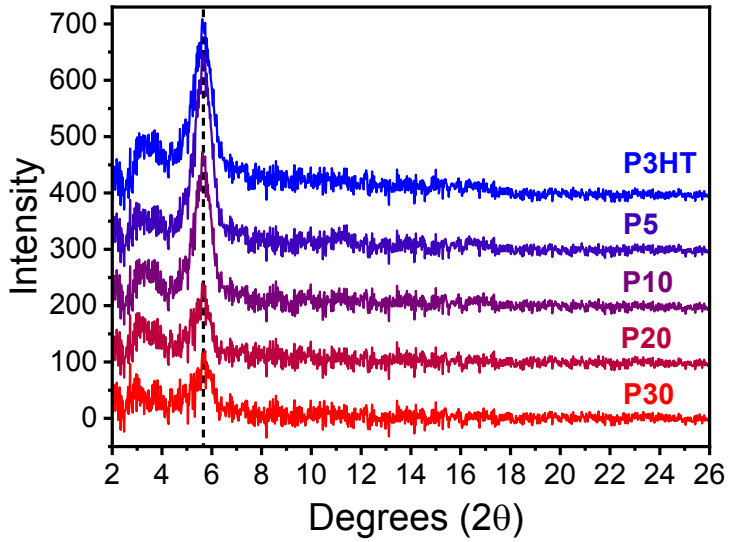

Figure S22. XRD of drop cast thin films polymer films baselined to blank silicon slide. Dotted line is to guide the reader to the peak showing the d(100) spacing.

Table S4. Table showing the d(100) spacing calculated using Braggs law from the XRD of drop cast polymer thin films.

Polymer	d(100) spacing (Å)[a]
P3HT	15.71
P5	15.60
P10	15.60
P20	15.55
P30	15.55

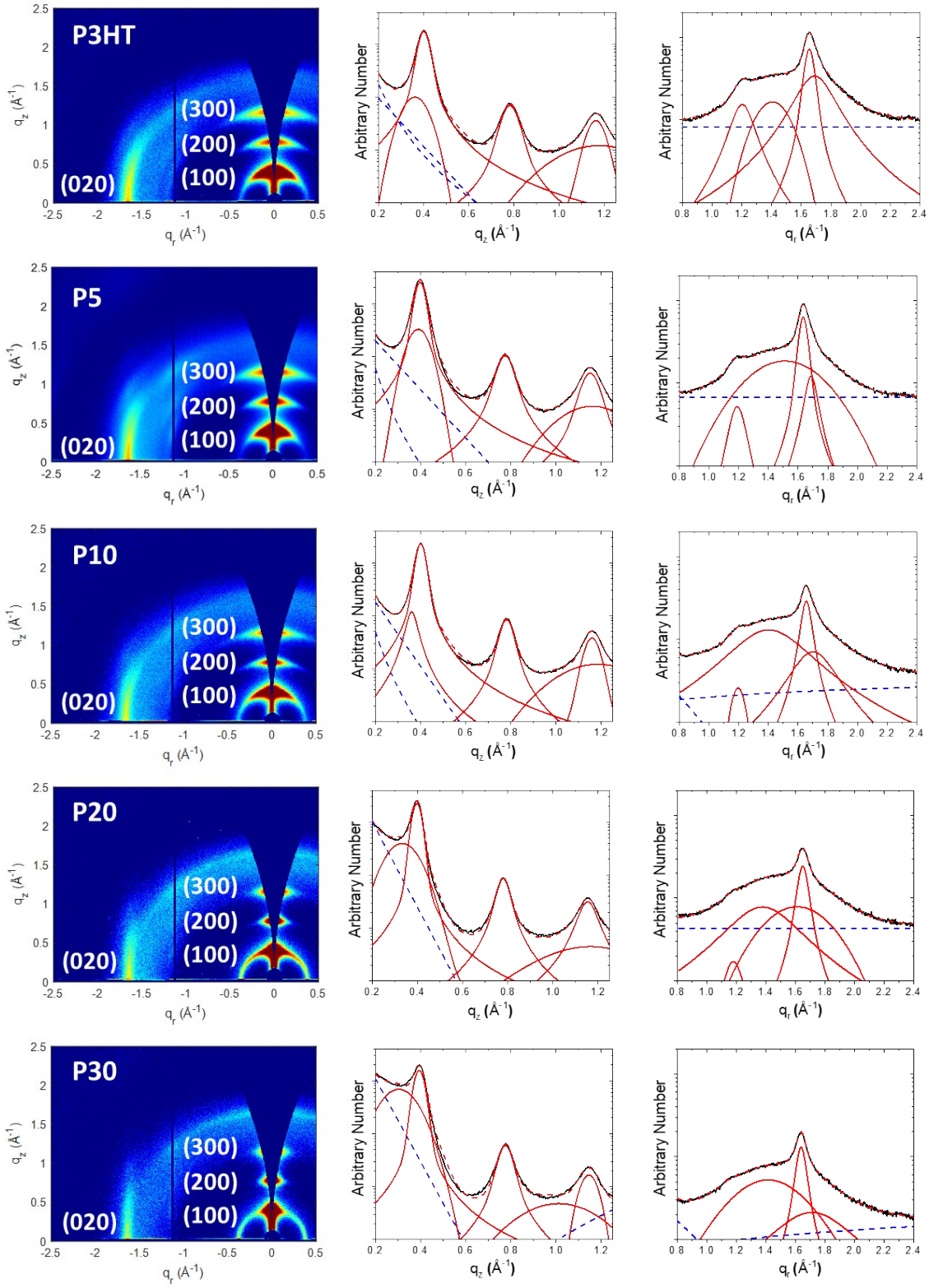

Figure S23. 2D GIWAXS patterns (left) of undoped spin cast polymer films. The d(100), d(200), d(300) and d(010) spacings are shown on these patterns. Fitted peak for (100), (200) and (300) peaks of out of plane line cuts (middle) and (010) peak of in plane line cuts (right) of undoped spin cast polymers.

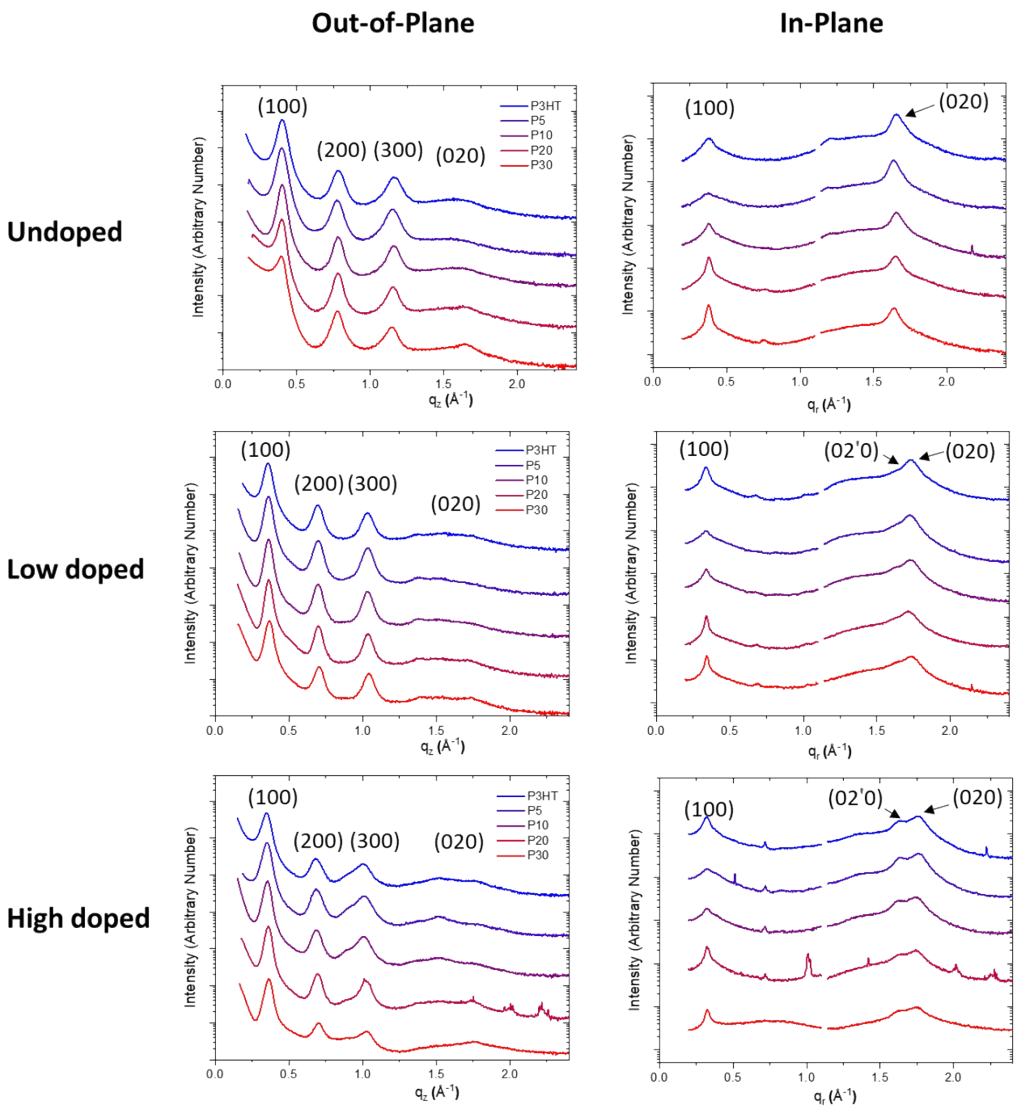

Figure S24. Out of plane (left) and in plane (right) line cuts of undoped (up), low doped (middle) and high doped (down) spin cast polymer films from 2D GIWAXS patterns.

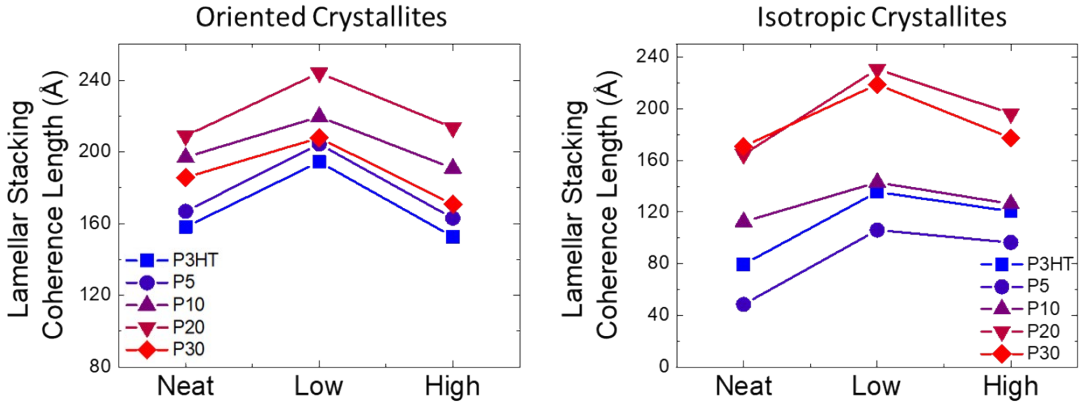

Figure S25. The lamellar coherence length change of P3HT:P3MEEMT copolymers with different composition and doping level of the oriented crystallites (left) and the isotropic crystallites (right).

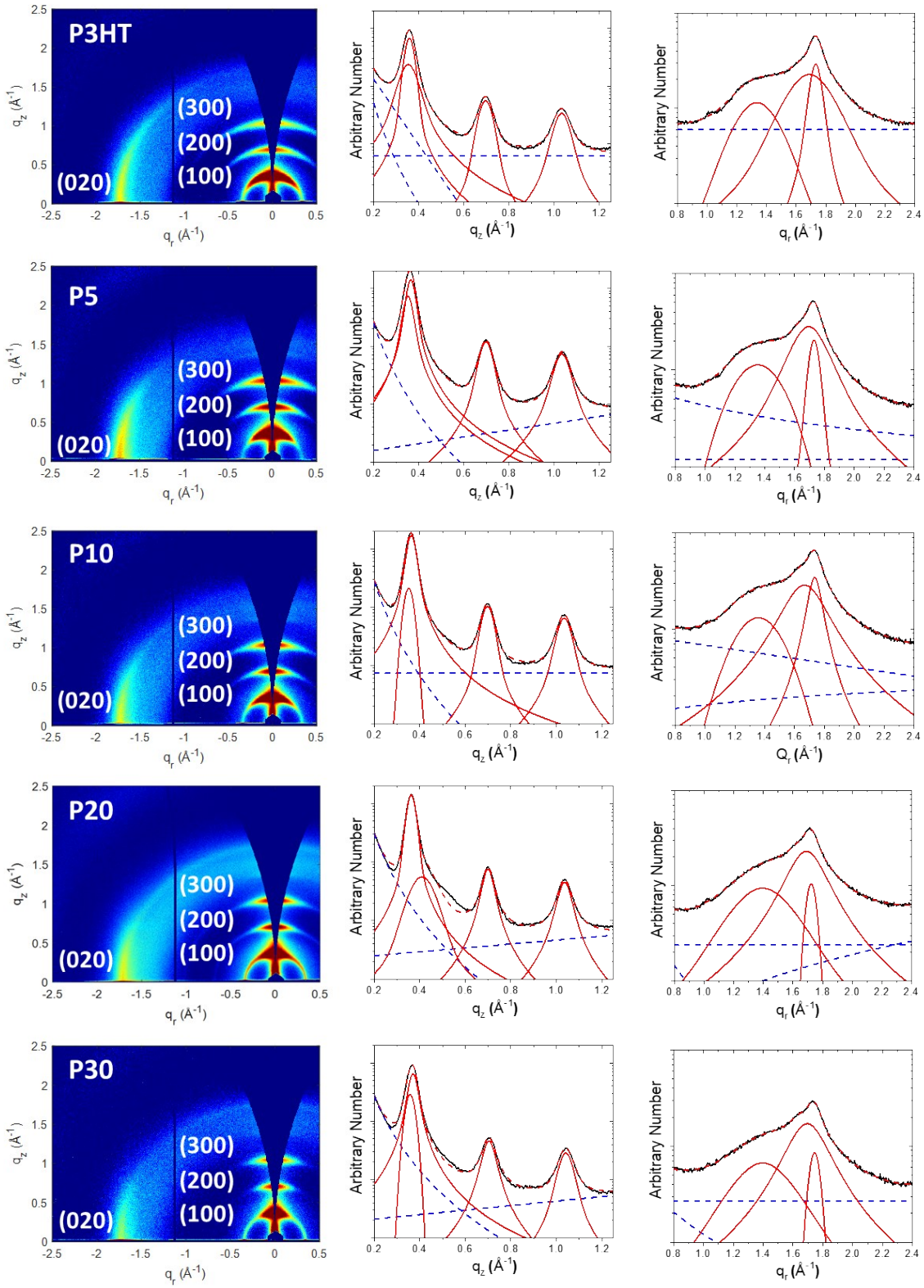

Figure S26. 2D GIWAXS patterns (left) of low doped spin cast polymers. The d(100), d(200), d(300) and d(010) spacings are shown on these patterns. Fitted peak for (100), (200) and (300) peaks of out of plane line cuts (middle) and (010) peak of in plane line cuts (right) of low doped spin cast polymers.

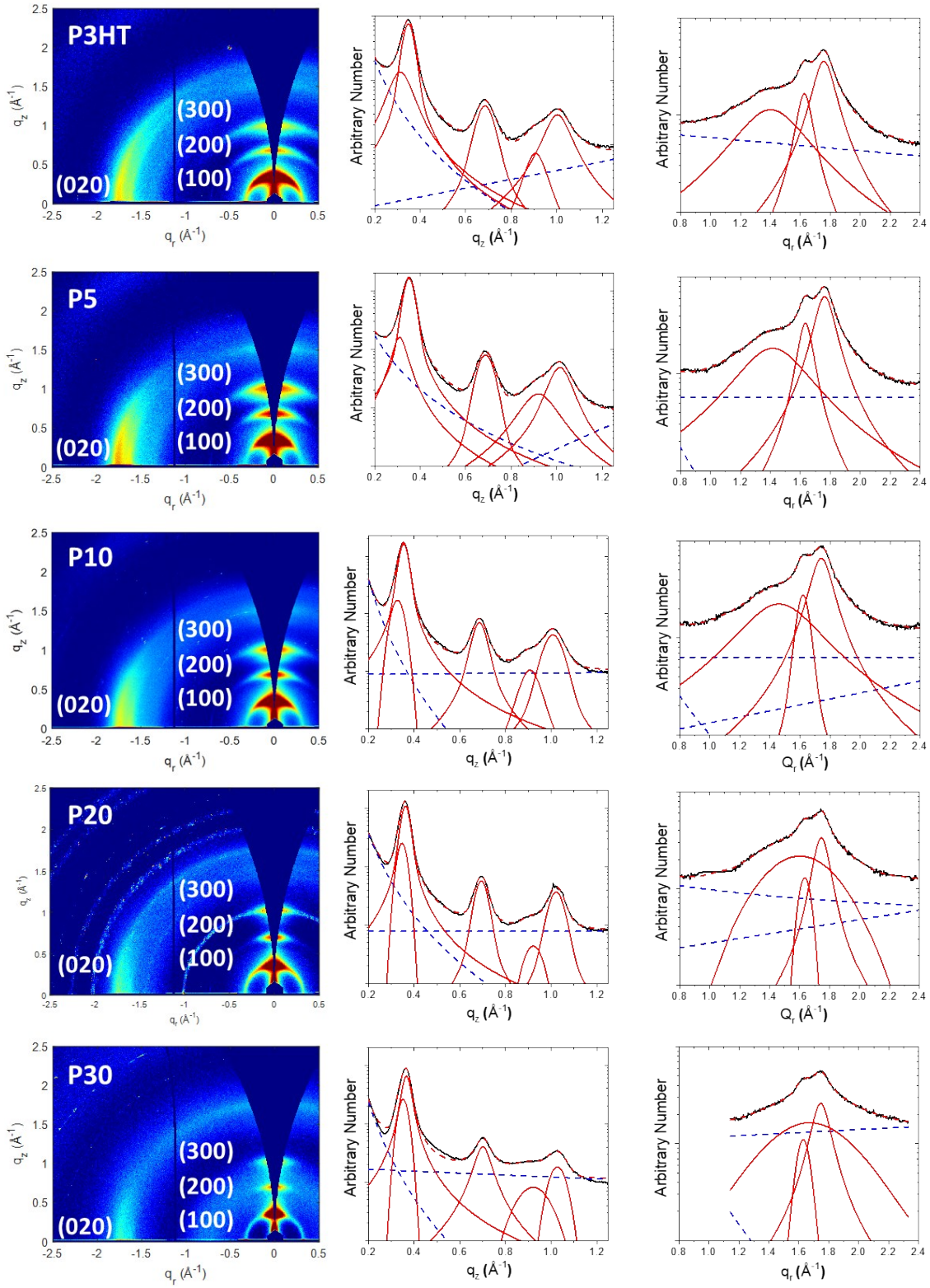

Figure S27. 2D GIWAXS patterns (left) of high doped spin cast polymer films. The d(100), d(200), d(300) and d(010) spacings are shown on these patterns. Fitted peak for (100), (200) and (300) peaks of out of plane line cuts (middle) and (010) peak of in plane line cuts (right) of high doped spin cast polymer films.

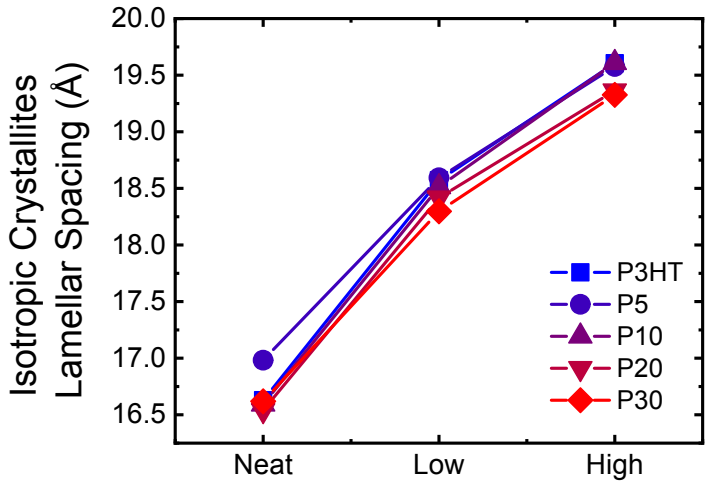

Figure S28. Lamellar stacking distance (d(100)) of isotropic crystallites from GIWAXS measurements of as-cast (from 10 mg/ml ODCB), low doped and high doped polymer thin films.

Table S5. Lamellar spacing extracted from 2-D GIWAXS pattern of polymers in different composition and doping level.

Lamellar Spacing (h00) (Å)	**P3HT**	**P5**	**P10**	**P20**	**P30**
$d_{Neat,\ Oriented}$[a]	16.1	16.2	16.1	16.1	16.2
$d_{Low\ doped,\ Oriented}$[a]	18.1	18.0	18.0	18.0	17.9
$d_{High\ doped,\ Oriented}$[a]	18.4	18.3	18.3	18.1	17.9
$d_{Neat,\ Isotropic}$[b]	-	17.0	16.6	16.5	16.6
$d_{Low\ doped,\ Isotropic}$[b]	-	18.6	18.5	18.4	18.3
$d_{High\ doped,\ Isotropic}$[b]	-	19.6	19.6	19.4	19.3

[a]Calculated from (200). [b]Calculated from (100).

Table S6. π - π spacing extracted from 2-D GIWAXS pattern of polymers in different composition and doping level.

π – π Spacing (010) (Å)	**P3HT**	**P5**	**P10**	**P20**	**P30**
$d_{Neat,\ Oriented}$	3.80	3.84	3.80	3.81	3.84
$d_{Low\ doped,\ Oriented}$[a]	3.63(3.72)	3.63(3.71)	3.62(3.77)	3.65(3.72)	3.60(3.71)
$d_{High\ doped,\ Oriented}$[a]	3.58(3.86)	3.57(3.85)	3.61(3.88)	3.60(3.84)	3.60(3.86)
$d_{Neat,\ Isotropic}$	3.81	3.98	3.90	3.81	3.81
$d_{Low\ doped,\ Isotropic}$	3.71	3.80	3.69	3.68	3.64
$d_{High\ doped,\ Isotropic}$	3.59	3.56	3.60	3.60	3.60

[a]π-stacking d-spacing of expanded π-stacking polymorph shown in parentheses.

2.8. Atomic Force Microscopy (AFM)

AFM was measured on spin cast thin films on quartz microscope slides from 10 mg/ml polymer solutions in ODCB dissolved at 80 °C. Solutions were spun at 2000 rpm for 90 secs then 8000 rpm for 30 secs from 80 °C in air on a Laurell Technologies Corporation Model WS-650MZ-23NPPB spin coater. Quartz slides were cleaned by sonicating in soapy water, DI water, acetone, and IPA for 15 mins. Prior to spin coating substrates were plasma cleaned using a Harrick Plasma PDC-32G Plasma Cleaner for 30 mins. AFM was carried out in air using a Bruker Dimension Icon system. ScanAsyst Air tips were used to image the samples in PeakForce Quantitative Nanomechanical Property Mapping (QNM) mode. Roughness was calculated using Nanoscope Analysis software.

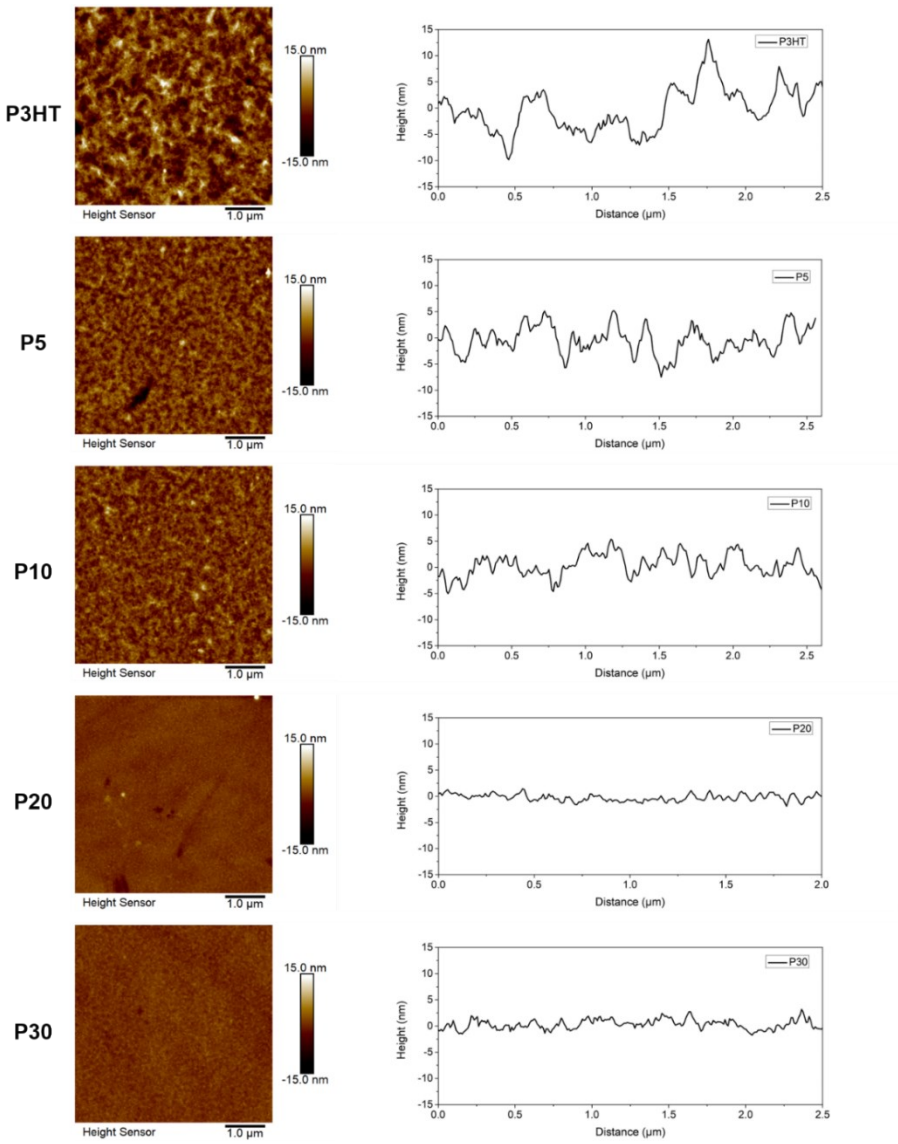

Figure S29. AFM images of spin cast polymer films. Representative height profiles are shown to the right of each image.

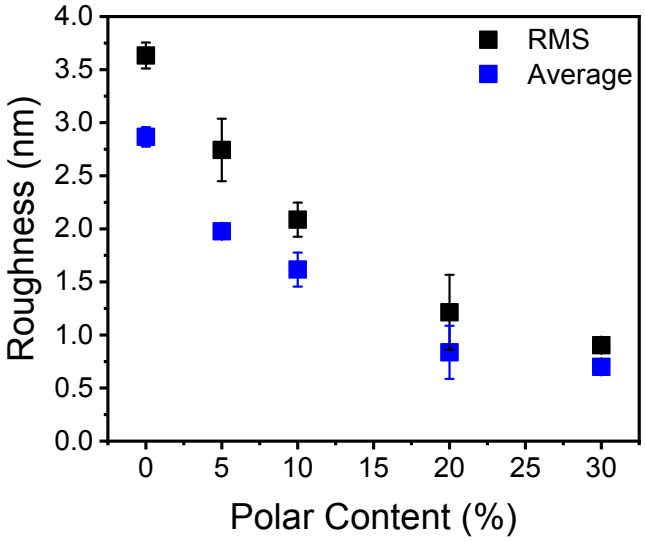

Figure S30. Plot of the average and route mean square (RMS) roughness of AFM images against polar content. Error bars come from the average of three measurements per image.

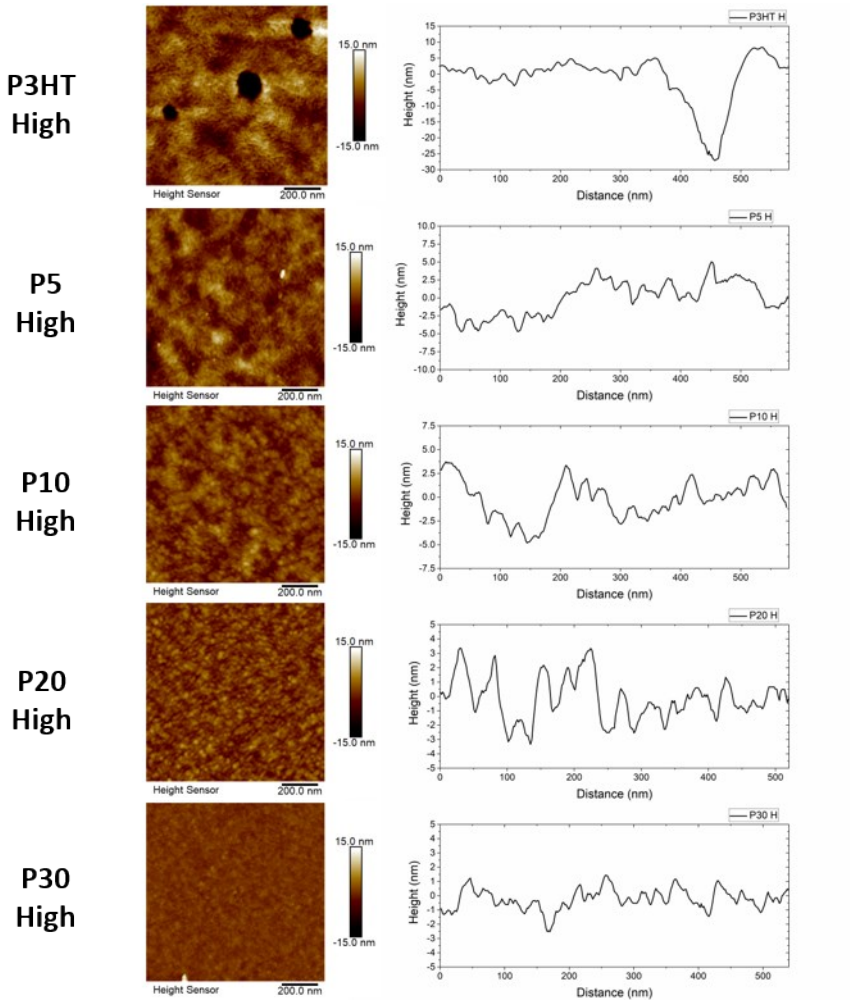

Figure S31. AFM images of spin cast polymer films doped with F4TCNQ at high doping conditions. Representative height profiles are shown to the right of each image.

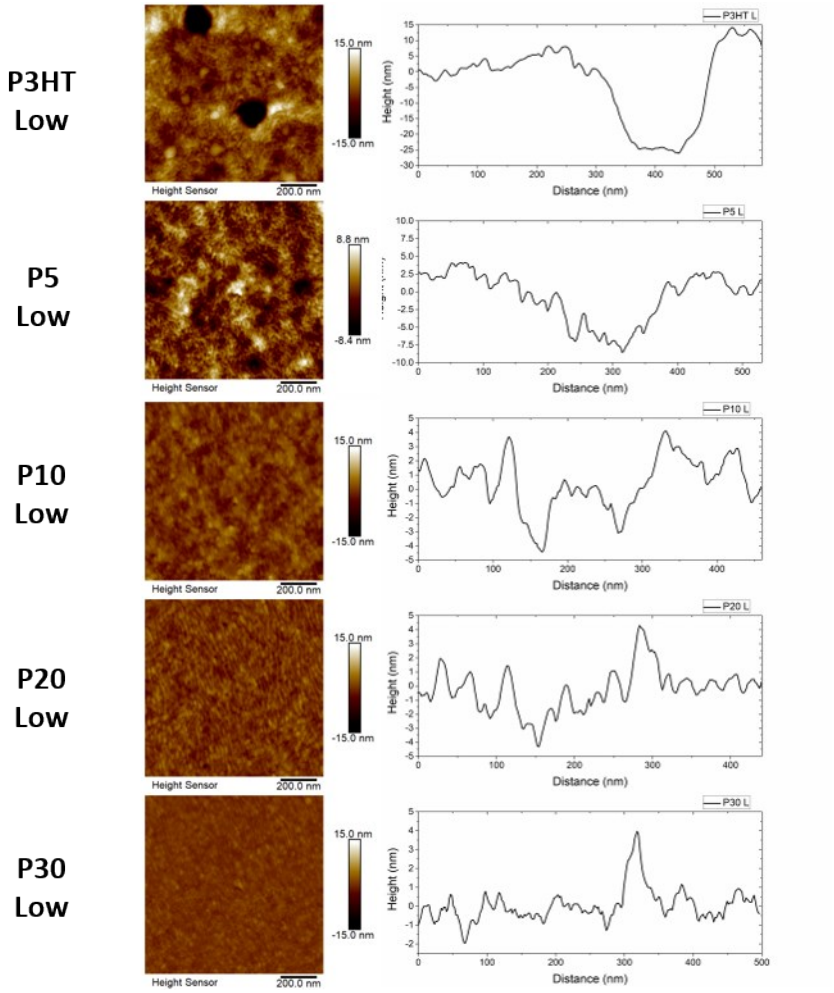

Figure S32. AFM images of spin cast polymer films doped with F4TCNQ at low doping conditions. Representative height profiles are shown to the right of each image.

2.9. Organic Field Effect Transistors (OFET)

Output and transfer characteristics were measured using top gate bottom contact device architecture with a 20 µm and 1 mm channel length and width respectively (W/L ratio of 50). Source and drain electrodes were gold, CYTOP as the insulating layer (~500 nm) and aluminium as the gate electrode. Insulating layer was annealed at 80 °C for 10 secs. Polymer thin films were spun at 1500 rpm for 60 seconds from 10 mg/ml ODCB solutions at 90 °C, then annealed at 150 °C for 1 hr and finally exposed to oxygen for 24 hrs. All measurements and fabrication were conducted under a nitrogen atmosphere unless otherwise stated. Measurements were performed on a Karl Suss probe station inside a nitrogen glovebox (Belle Technologies, <20 ppm O_2) using an Agilent 4155B sourcemeter controlled by a custom LabView program.

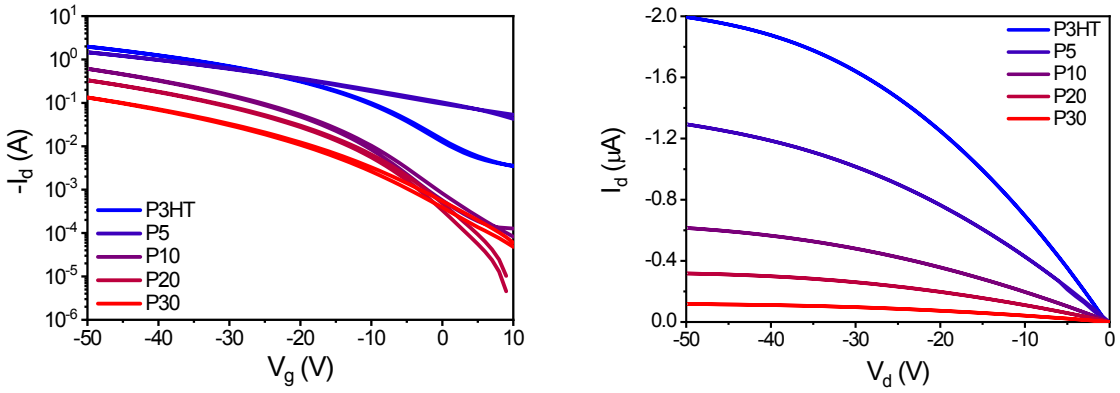

Figure S33. Transfer (left) and output (right) curve of OFETs at a -50 V gate and drain voltage, respectively.

Table S7. Table showing the saturation field effect hole mobilities and the on/off ratio from the OFET measurements.

Polymer	Field effect hole mobility $x10^{-3}$ cm^2 V^{-1} s^{-1}	On/Off Ratio
P3HT	3.8	5 x 10^2
P5	2.3	2 x 10^1
P10	2.1	6 x 10^3
P20	1.1	4 x 10^4
P30	0.5	2 x 10^3

2.10. Characterisation and Conductivity Measurements of Doped Thin Films

CaF_2 substrates (1 cm square, 1 mm thick, Crystran Ltd.) patterned with van der Pauw contacts (1mm contacts at each corner) was chosen to permit conductivity, UV-vis, and FTIR measurements on a single sample. Substrates were first prepatterned with Cr/Au electrodes (5/25 nm) by thermal evaporation through a shadow mask, then cleaned by sequential sonication in Decon 90, DI water, acetone, and isopropanol, dried under nitrogen flow, and exposed to oxygen plasma for 10 minutes. After transferring to a nitrogen glovebox (MBraun Labmaster 130, <1 ppm H_20, O_2), polymer thin films were spun cast at 1500 rpm for 60 secs (Specialty Coating Systems G3P) from 10 mg/ml ODCB solutions at 80 °C, then annealed at 180 °C for 20 mins under N_2. Thin films were doped with two different concentrations under nitrogen atmosphere. High doping was carried out by depositing a 1 mg/ml solution of F4TCNQ in MeCN, leaving on the films for 60 seconds, then removed via spinning at 8000 rpm for 30 seconds. This was followed by another 1 mg/ml solution of F4TCNQ in ODCB leaving on the

film for 120 seconds, then removed by spinning at 8000 rpm for 30 seconds. Low doping was carried out via depositing a 0.1 mg/ml solution of F4TCNQ in MeCN, leaving on for 10 secs, then spinning off at 8000 rpm for 30 secs. After initial conductivity and spectroscopy measurements, the doped films were annealed under nitrogen at 80 °C for 20 mins on a hotplate and conductivity was remeasured. The **P20** low doping annealed sample was removed from the thermal stability dataset due to a scratch during sample handling after the initial conductivity measurement, which prevented an accurate measurement after annealing. Film thickness was measured using a Bruker DekTak XT.

UV-Vis measurements were performed on a Shimadzu UV-3600i UV-vis-NIR spectrometer. IR spectroscopy was carried out on a Bruker Vertex 70v FT-IR spectrometer under vacuum using a DLaTGS detector. Thin film interference present in the data were filtered out in MATLAB using a stopband filter. Conductivity measurements were measured in a Karl Suss probe station under a nitrogen atmosphere (<20 ppm O_2) using an Agilent 4155B sourcemeter following the standard van der Pauw method. Four I-V measurements of each sample were performed, corresponding to sourcing current between each pair of adjacent contacts, while measuring the voltage at the other pair of contacts. These data were checked for current reversal and reciprocity consistency to <5% variance, following NIST recommendations; the van der Pauw equation was then used to determine the sheet conductivity.[6] Solution UV-Vis of KF4TCNQ was carried out on a Shimadzu UV3600 UV-Vis-NIR spectrometer in 10 mm path length quartz cuvettes.

Table S8. Thickness measurements of polymer thin films spun from 10 mg/ml ODCB solutions at 80 °C at 1500 rpm for 60 secs.

Polymer	Average (nm)	Error (nm)
P3HT	53.2	± 0.5
P5	49.5	± 2.4
P10	34.2	± 1.6
P20	76.9	± 6.6
P30	41.9	± 5.5

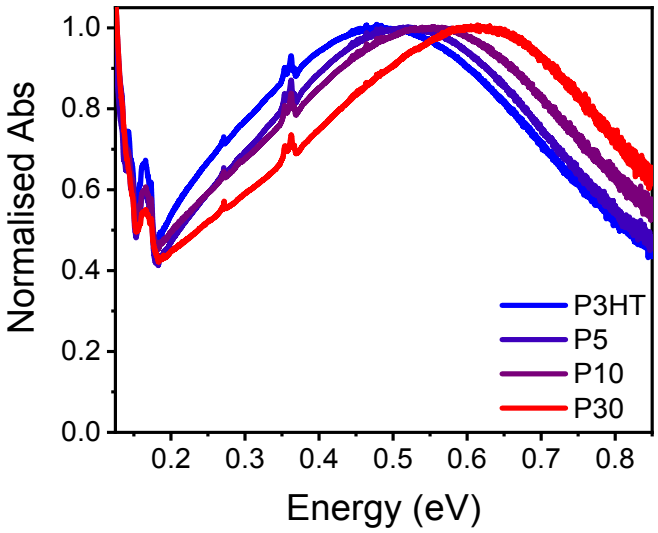

Figure S34. Normalised FTIR spectra of low doped polymer films. FTIR is normalised to the P1 polaron peak.

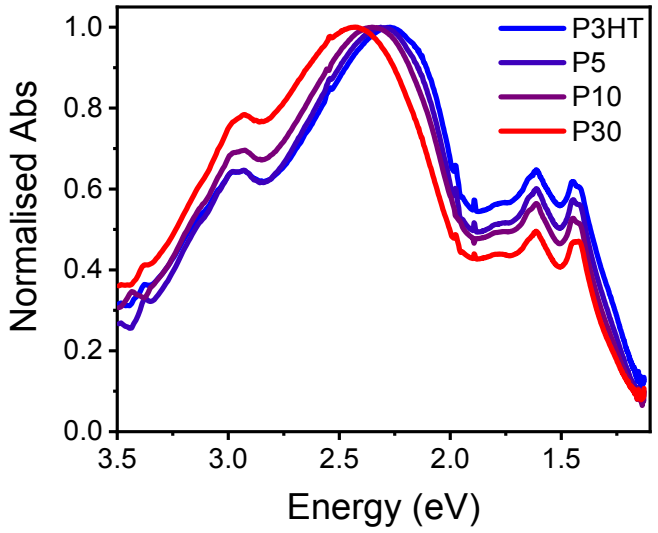

Figure S35. Normalised UV-Vis spectra of low doped polymer films. UV-Vis is normalised to the π-π* absorption peak.

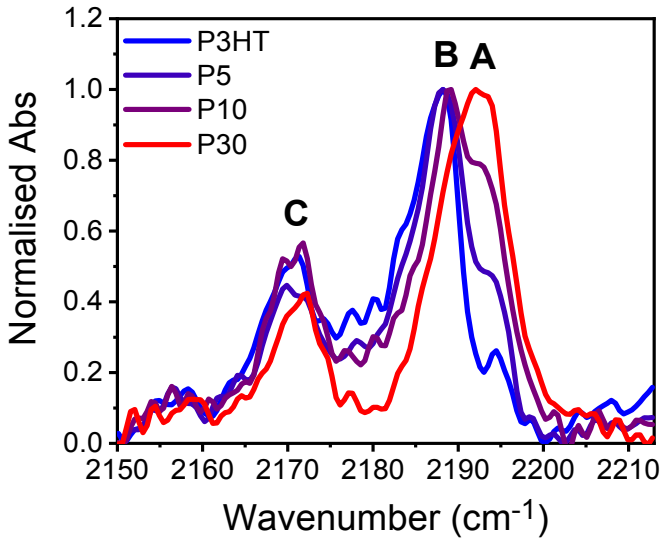

Figure S36. FTIR spectra between 2150 – 2213 cm^{-1}, where the vibrations of CN on F4TCNQ can be observed, for low doping of polymer films. Spectra are normalised to λ_{max} and A, B and C indicate the notable peaks at 2194, 2187 and 2169 cm^{-1}, respectively.

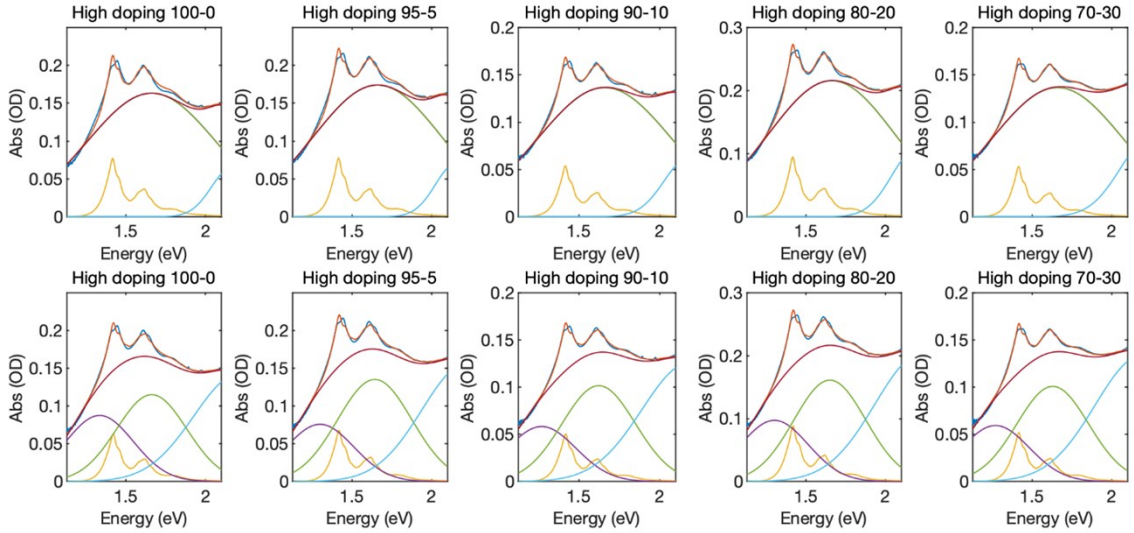

Figure S37. Fitted normalised thin film UV-Vis spectra of high doped polymer thin films (P3HT (labelled 100-0, **P5** (95-5), **P10** (90-10), **P20** (80-20) and **P30** (70-30)) using two baseline methods. The top row uses the sum of two Gaussian curves as the baseline, one as the π-π* absorption edge and the other polaron peak. The bottom row uses the sum of three Gaussian curves as the baseline, using peak positions obtained from the literature, one as the π-π* absorption edge and two polaron peaks.[7] The F4TCNQ spectrum was obtained from solution UV-Vis of KF4TCNQ in acetonitrile. The lines in each spectrum are the measured spectrum (dark blue), total fit (orange), baseline (sum of Gaussians, red), F4TCNQ anion (yellow), polaron (green and purple), π-π * edge (light blue).

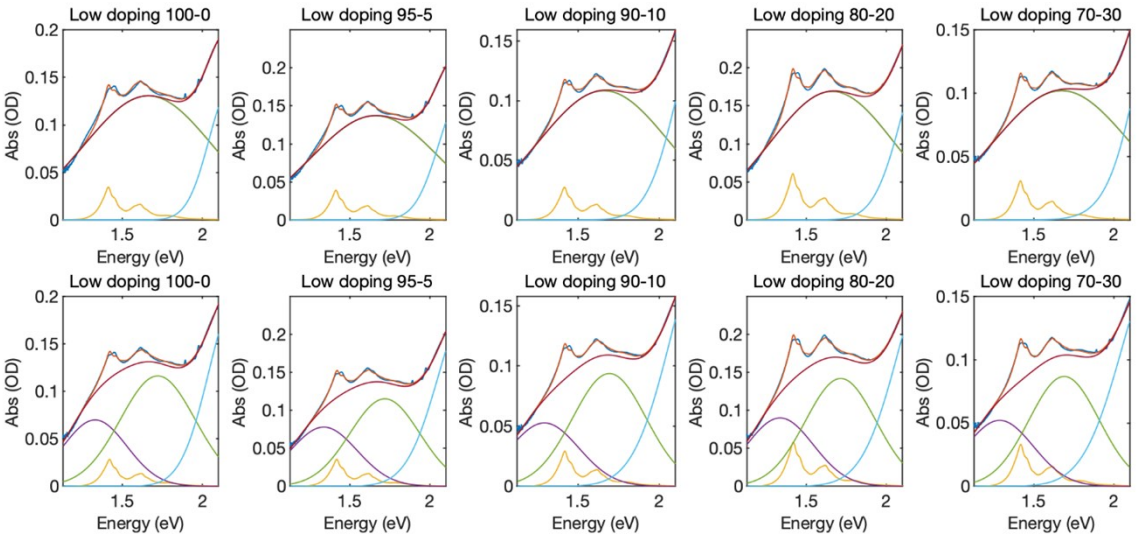

Figure S38. Fitted normalised thin film UV-Vis spectra of low doped polymer thin films (P3HT (labelled 100-0, **P5** (95-5), **P10** (90-10), **P20** (80-20) and **P30** (70-30)) using two baseline methods. The top row uses the sum of two Gaussian curves as the baseline, one as the π-π* absorption edge and the other polaron peak. The bottom row uses the sum of three Gaussian curves as the baseline, using peak positions obtained from the literature, one as the π-π* absorption edge and two polaron peaks.[7] The F4TCNQ spectrum was obtained from solution UV-Vis of KF4TCNQ in acetonitrile. The lines in each spectrum are the measured spectrum (dark blue), total fit (orange), baseline (sum of Gaussians, red), F4TCNQ anion (yellow), polaron (green and purple), π-π * edge (light blue).

Table S9. Estimations of the F4TCNQ anion concentration from fittings of the solid-state UV-Vis spectrum of doped polymer thin films.

Polymer	High Doping F4TCNQ Anion Concentration (cm^{-3})		Low Doping F4TCNQ Anion Concentration (cm^{-3})	
	2 Gaussians	3 Gaussians	2 Gaussians	3 Gaussians
P3HT	2.08×10^{20}	1.70×10^{20}	9.35×10^{19}	7.67×10^{19}
P5	2.25×10^{20}	1.97×10^{20}	1.13×10^{20}	1.03×10^{20}
P10	2.26×10^{20}	2.14×10^{20}	1.17×10^{20}	1.24×10^{20}
P20	1.77×10^{20}	1.65×10^{20}	1.14×10^{20}	1.09×10^{20}
P30	1.81×10^{20}	1.77×10^{20}	1.06×10^{20}	1.14×10^{20}

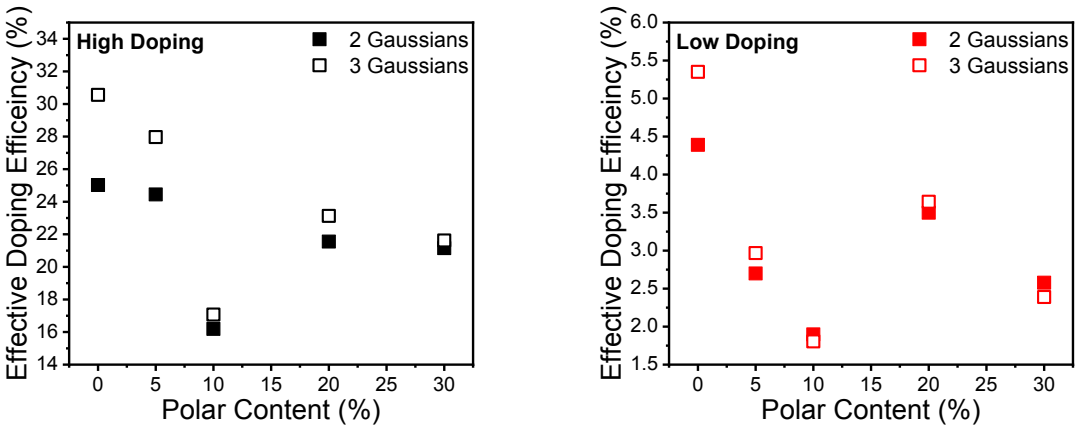

Figure S39. Plots of the effective doping efficiency (EDE) vs polar content for high (left) and low (right) doping conditions. The effective doping efficiency was calculated using the equation

$$EDE\ (\%) = \frac{\sigma_{measured}}{en_{anion}\mu_{FET}} x\ 100 \qquad (2)$$

where $\sigma_{measured}$ is the measured electrical conductivity of high and low doped polymer films (S cm^{-1}), n_{anion} is the fitted F4TCNQ anion concentration (cm^{-3}), μ_{FET} is the measured OFET hole mobility ($cm^2\ V^{-1}\ s^{-1}$) and e is the electron electric charge (1.602 x 10^{-19} C). It is important to distinguish the effective doping efficiency from the true doping efficiency, as the equation above makes several assumptions. First, it assumes the charge carrier concentration is equal to the F4TCNQ anion concentration, and that no fractional charge transfer complexes are formed. More critically, it assumes that the carrier mobility does not change with doping level. Mobility is usually assumed to be doping level dependent. However, because the doping level in each sample is similar, if we assume the variation of mobility with doping level is similar for each polymer, then at a given doping level the effective doping efficiency should reproduce the trend in the true doping efficiency. Therefore, the effective doping efficiency should give a reasonable estimate of whether the doping efficiency is changing as polar sidechains are added, but the absolute magnitude of the doping efficiency should not be considered quantitative.

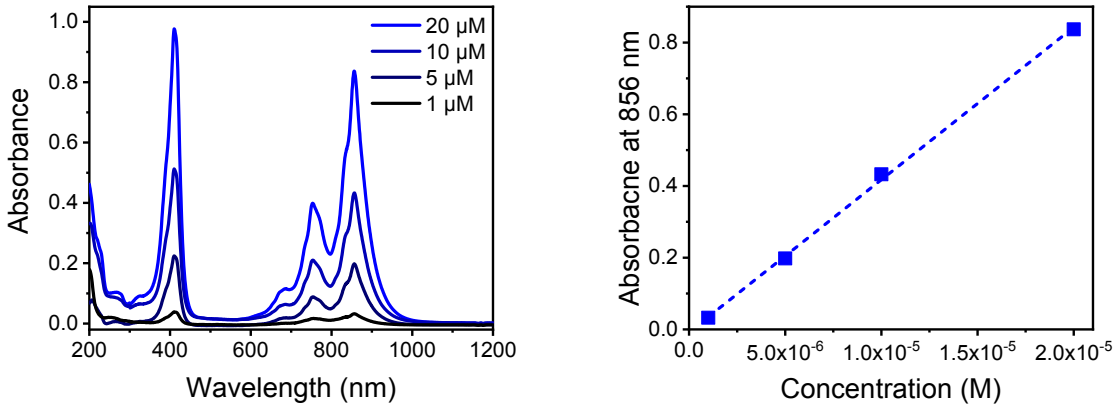

Figure S40. Solution spectrum of KF4TCNQ in acetonitrile at different concentrations (left) and a calibration curve of absorbance of KF4TCNQ at 856 nm vs concentration (right). From the gradient of the fitted straight line the absorption coefficient was calculated to be 42 x 10^3 M^{-1} cm^{-1}.

3. References

1 C. K. Song, B. J. Eckstein, T. L. D. Tam, L. Trahey and T. J. Marks, *ACS Applied Materials and Interfaces*, 2014, **6**, 19347–19354.

2 A. A. Y. Guilbert, M. Zbiri, P. A. Finn, M. Jenart, P. Fouquet, V. Cristiglio, B. Frick, J. Nelson and C. B. Nielsen, *Chemistry of Materials*, 2019, **31**, 9635–9651.

3 D. Kiefer, R. Kroon, A. I. Hofmann, H. Sun, X. Liu, A. Giovannitti, D. Stegerer, A. Cano, J. Hynynen, L. Yu, Y. Zhang, D. Nai, T. F. Harrelson, M. Sommer, A. J. Moulé, M. Kemerink, S. R. Marder, I. McCulloch, M. Fahlman, S. Fabiano and C. Müller, *Nature Materials*, 2019, **18**, 149–155.

4 K. Tremel and S. Ludwigs, *P3HT Revisited – From Molecular Scale to Solar Cell Devices*, Springer US, 2014, vol. 265.

5 Z. Jiang, *Journal of Applied Crystallography*, 2015, **48**, 917–926.

6 Resistivity and Hall Measurements, https://www.nist.gov/pml/nanoscale-device-characterization-division/popular-links/hall-effect/resistivity-and-hall. (accessed Spet. 2020)

7 C. Wang, D. T. Duong, K. Vandewal, J. Rivnay and A. Salleo, *Physical Review B - Condensed Matter and Materials Physics*, 2015, **91**, 1–7.